

Article

Timing of Transition from Proto- to Paleo-Tethys: Evidence from the Early Devonian Bimodal Volcanics in the North Qaidam Tectonic Belt, Northern Tibetan Plateau

Mao Wang ¹, Xianzhi Pei ^{1,2,*}, Ruibao Li ^{1,2}, Lei Pei ^{1,2}, Zuochen Li ^{1,2} , Chengjun Liu ^{1,2}, Lili Xu ^{1,2} and Hao Lin ¹

¹ Key Laboratory of Western China's Mineral Resources and Geological Engineering, Ministry of Education, School of Earth Science and Resources, Chang'an University, Xi'an 710054, China;

wmchd_0908@163.com (M.W.); liruibao0971@163.com (R.L.); peilei.1989@163.com (L.P.);

lizuoichen@chd.edu.cn (Z.L.); lchjchd@126.com (C.L.); lily203@126.com (L.X.); linhao231@163.com (H.L.)

² Key Laboratory for Mineralization and Efficient Utilization of Critical Metals, Xi'an 710054, China

* Correspondence: peixzh@chd.edu.cn

Abstract: The transition from the Proto- to the Paleo-Tethys is still a controversial issue. This study reports a new petrology, zircon U–Pb geochronology, and whole-rock geochemistry of volcanic rocks from the Maoniushan Formation in the Nankeke area, northern Qaidam (NQ) of the Tibetan Plateau, to provide new evidence for the transition from the Proto- to the Paleo-Tethys oceans. The volcanic suite consists mainly of rhyolitic crystal lithic tuff lavas and minor basalts. Zircon U–Pb data indicate that the bimodal volcanic rocks were formed during the Early Devonian (ca. 410–409 Ma). Geochemically, the basalts have low contents of SiO₂ (48.92 wt.%–51.19 wt.%) and relatively high contents of MgO (8.94 wt.%–9.99 wt.%), TiO₂ (1.05 wt.%–1.29 wt.%), K₂O (2.35 wt.%–4.17 wt.%), and K₂O/Na₂O ratios (1.04–2.56), showing the characteristics of calc-alkaline basalts. Their rare earth element (REE) patterns and trace element spider diagrams are characterized by enrichments in LREEs (LREE/HREE = 18.31–21.34) and large ion lithophile elements (LILEs; Rb, Th, and K) and depletion in high-field-strength elements (HFSEs; Nb, Ta, P, and Ti), with slight negative Eu anomalies (Eu/Eu* = 0.82–0.86), which are similar to Etendeka continental flood basalts (CFB). These features suggest that the basalts were most likely derived from low degree (1%–5%) partial melting of the asthenospheric mantle, contaminated by small volumes of continental crust. In contrast, the felsic volcanics have high SiO₂ (68.41 wt.%–77.12 wt.%), variable Al₂O₃ (9.56 wt.%–12.62 wt.%), low MgO, and A/CNK ratios mostly between 1.08 and 1.15, defining their peraluminous and medium-K calc-alkaline signatures. Their trace element signatures show enrichments of LREEs and LILEs (e.g., Rb, Th, U, K, and Pb), depletion of HFSEs (e.g., Nb, Ti, Ta, and P), and negative Eu anomalies (Eu/Eu* = 0.22–0.66). These features suggest that the felsic volcanics were derived from partial melting of the middle crust, without interaction with mantle melts. Considering all the previous data and geochemical features, the Maoniushan Formation volcanic rocks in NQ formed in a post-collisional extensional setting associated with asthenospheric mantle upwelling and delamination in the Early Devonian. Together with the regional data, this study proposed that the Proto-Tethys Ocean had closed and evolved to the continental subduction/collision orogeny stage during the Middle to Late Ordovician, evolved to the post-collisional extensional stage in the Early Devonian, and finally formed the Zongwulong Ocean (branches of the Paleo-Tethys Ocean) in the Late Carboniferous, forming the tectonic framework of the Paleo-Tethys Archipelagic Ocean in the northern margin of the Tibetan Plateau.



Citation: Wang, M.; Pei, X.; Li, R.; Pei, L.; Li, Z.; Liu, C.; Xu, L.; Lin, H. Timing of Transition from Proto- to Paleo-Tethys: Evidence from the Early Devonian Bimodal Volcanics in the North Qaidam Tectonic Belt, Northern Tibetan Plateau. *Minerals* **2023**, *13*, 532. <https://doi.org/10.3390/min13040532>

Academic Editor: Sung Hi Choi

Received: 24 February 2023

Revised: 29 March 2023

Accepted: 7 April 2023

Published: 10 April 2023



Copyright: © 2023 by the authors. Licensee MDPI, Basel, Switzerland. This article is an open access article distributed under the terms and conditions of the Creative Commons Attribution (CC BY) license (<https://creativecommons.org/licenses/by/4.0/>).

Keywords: bimodal volcanic rocks; Maoniushan Formation; Northern Qaidam; post-collisional extensional setting; Proto-Tethys; Paleo-Tethys

1. Introduction

The Northern Qaidam (NQ) tectonic belt is located at the junction of the Central Orogenic Belt along the northern margin of the Tibetan Plateau, which is an important part of the Paleozoic orogenic system along the northern margin of the Tibetan Plateau [1–5]. The NQ is a Paleozoic subduction/collision complex belt that has undergone complicated orogeny and includes at least two stages of Tethys Ocean-related tectonic cycles, namely, the Early Paleozoic Proto-Tethys tectonic cycle and the Late Paleozoic to Early Mesozoic Paleo-Tethys tectonic cycle, which is one of the key areas for studying the Proto- and Paleo-Tethys Ocean tectonic transition [2,4–20].

Previous data show that the Proto-Tethys Ocean in the NQ began to subduct northward during the Early to Middle Cambrian, producing long-lived voluminous arc-related magmatic rocks [5,10,17,21–23]. In the Middle and Late Ordovician, the Qaidam Block was dragged to initiate deep subduction, evolved to a continental subduction/collision orogeny stage, and then evolved to a post-orogenic collapse stage around the Late Silurian [4,5,14–17,24–28]. The Maoniushan Formation molasses deposits, which are widely exposed in the NQ, represent the end of the Proto-Tethys tectonic cycle and the beginning of the Paleo-Tethys tectonic cycle [29–31]. The NQ records the complete formation and evolution of the Proto-Tethys Ocean, which many researchers have focused on. However, the details of the transition from the Proto- to Paleo-Tethys and the aspects of the opening of the Paleo-Tethys Ocean are still uncertain. Moreover, the petrogenesis of Permian to Middle Triassic arc-related magmatic rocks in the NQ also leads to different viewpoints on the existence of the Paleo-Tethys Ocean [32–43]. Most scholars have argued for the existence of the Late Hercynian–Indosinian Zongwulong Ocean, and these rocks are considered as a response to the southward subduction of the Zongwulong Ocean [32–38]. Other scholars have suggested that the NQ experienced an intracontinental rift during the Late Hercynian to Indosinian and did not form an ocean basin, and the arc magmatic rocks of this period are a remote response to the northward subduction of the Paleo-Tethys Ocean (A'nyemaqen–Buqingshan Ocean) [39–43].

In general, bimodal volcanic rocks are mainly composed of basalt and rhyolite, which are commonly considered to be generated in extensional environments, such as continental rifts, back-arc basins, and post-orogenic extensional settings [44–50]. In addition, slab break-off [51], lithospheric delamination [52–54], and asthenospheric mantle convection erosion [55] can induce partial melting of the lithospheric mantle and/or asthenosphere mantle and crust to form bimodal volcanic rocks. Therefore, these rocks are very important for understanding the tectonic transition of continental orogeny from compression to extension and for exploring the mechanism of the post-orogenic collapse stage.

This paper focuses on bimodal volcanic rocks from the Maoniushan Formation in the Nankeke area in the eastern segment of the NQ and present petrological, zircon U–Pb geochronological, and geochemical data, together with detailed field investigations, to determine the emplacement ages, petrogenesis, and tectonic setting of the bimodal volcanic rocks and to provide new constraints on the tectonic transition of the Proto- to Paleo-Tethys Ocean of the NQ.

2. Geological Setting

The NQ is located on the northern margin of the Tibetan Plateau and is part of the Central Orogenic System or the Qinling–Qilian–Kunlun Orogenic System. It extends for more than 400 km to the NNW from the Wahongshan–Wenquan fault in the east to the Altyn–Tagh fault in the west and is bounded by the Qilian Orogen and the Qaidam Block in the north and the south, respectively (Figure 1a,b). From north to south, the NQ contains three tectonic units, namely, the Zongwulong Tectonic Belt, Olongbuluke Block (OB), and North Qaidam Ultrahigh/High-Pressure (UHP/HP) Metamorphic Belt, which are separated by the Zongwulong fault and Olongbuluke–Maoniushan fault, respectively (Figure 2) [2,4,9,14,56–65]. The Zongwulong Tectonic Belt stratigraphically incorporates the Carboniferous–Permian Zongwulong Group and the Early–Middle Triassic Longwuhe

and Gulangdi Formations [35,66]. The OB consists of a Precambrian metamorphic basement, including the Paleoproterozoic Delingha Complex, the Paleoproterozoic Dakendaban Group, and the Mesoproterozoic Wandonggou Group, unconformably overlaid by the Nanhua–Sinian QuANJI Group and the volcanic sedimentary sequences since the Early Paleozoic [56,61,67,68]. The North Qaidam Ultrahigh/High-Pressure (UHP/HP) Metamorphic Belt, which consists of the Paleoproterozoic Dakendaban Group, the Mesoproterozoic Shaliuhe Group, the Early Paleozoic Tanjianshan Group, mafic–ultramafic rocks, and ophiolitic mélangé, contains numerous metamorphic rocks [12,13,69]. These metamorphic rocks are composed predominantly of orthogneiss, paragneiss, minor eclogite, and garnet peridotite. Previous zircon U–Pb ages show that the gabbro of the ophiolite formed between 535 and 496 Ma, recording the initial deep subduction of the oceanic crust [23,70–72]. The metamorphic ages of the eclogite at 460–420 Ma represent the UHP/HP metamorphic event in the NQ [12,13,43], while the Early Paleozoic granites indicate that the subduction/collision-related magmatism occurred at ca. 470–370 Ma [9,10,12,13,37,38,43].

The Maoniushan Formation is widely distributed in the Early Paleozoic post-orogenic molasses basin around the Qaidam Basin, specifically the Saishiteng–Amunike–Maoniushan Mountain in the NQ on the north side and the Shuinichang–Juchishan–Xiariha Basin in the East Kunlun orogenic belt on the south side. The Maoniushan Formation mainly contains the upper volcanic and the lower clastic rocks. The clastic rocks are composed of sandstone, siltstone, and glutenite, whereas the volcanic rocks consist mostly of basalt, dacite, rhyolite, and pyroclastic rocks. The Maoniushan Formation around the Qaidam Basin showed good consistency based on the lithological assemblages and stratigraphic contacts. Combining the ages of the volcanic rocks and plant fossils around the Qaidam Basin suggested that the Maoniushan Formation was formed in the Late Silurian to Late Devonian [73–78].

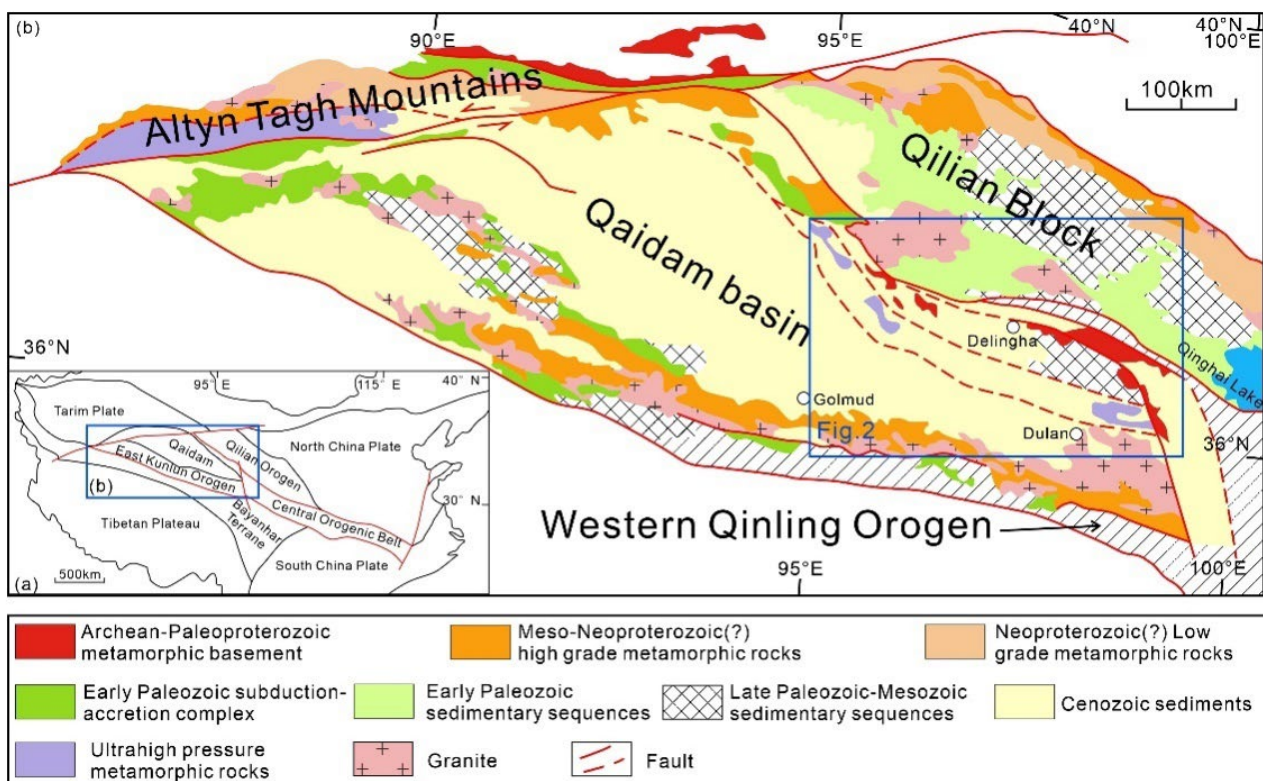


Figure 1. (a) Tectonic framework of the Central China Orogen [79]; (b) Simplified geological map of the NQ and the surrounding region [14].

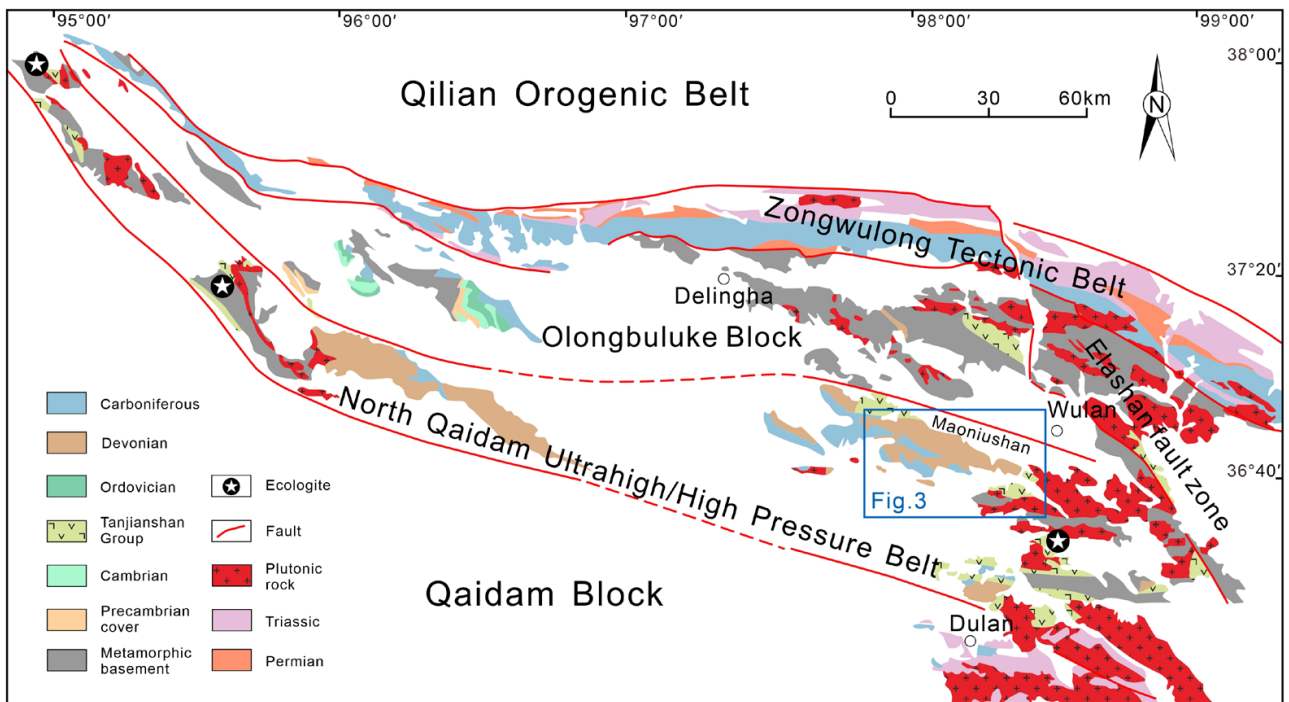


Figure 2. Diagram of the division of tectonic units in the NQ [80].

The study area is located in the Nankeke of the Maoniushan area of the eastern segment of the NQ, which stratigraphically mainly incorporates the Cambrian–Ordovician Tanjianshan Group, the Early Devonian Maoniushan Formation, the Lower Carboniferous Chengqianggou Formation, the Huaitoutala Formation, and the Upper Carboniferous Keluke Formation. The Paleoproterozoic Dakendaban Group, the Mesoproterozoic Shaliuhe Group, and the Lower Cretaceous Quanyagou Formation are locally exposed in this area (Figure 3, Table 1). The Paleoproterozoic Dakendaban Group is a Precambrian metamorphic basement that is a suite of mafic acid volcanic sedimentary formation. The Mesoproterozoic Shaliuhe Group is mainly composed of a suite of mafic–intermediate volcanic rocks and littoral neritic terrigenous clastic carbonatite rocks. The Cambrian–Ordovician Tanjianshan Group mainly consists of low-grade metamorphic volcanic sedimentary rocks, such as marble, metabasalt, andesite, schist, and siliceous rocks. The Carboniferous strata contain various types of limestones and clastic rocks, showing a series of upward-fining, littoral, neritic, terrigenous, clastic, carbonatite rocks (Table 1). Meso-Cenozoic sediments are unconformably overlaid by the above strata, and the exposed strata are mostly in fault or unconformity contact. Furthermore, the strata located in the southeast of this area have been invaded by Ordovician–Triassic plutons, and minor amounts of Paleoproterozoic Hudesheng gneiss and Middle Ordovician ultramafic rocks are exposed.

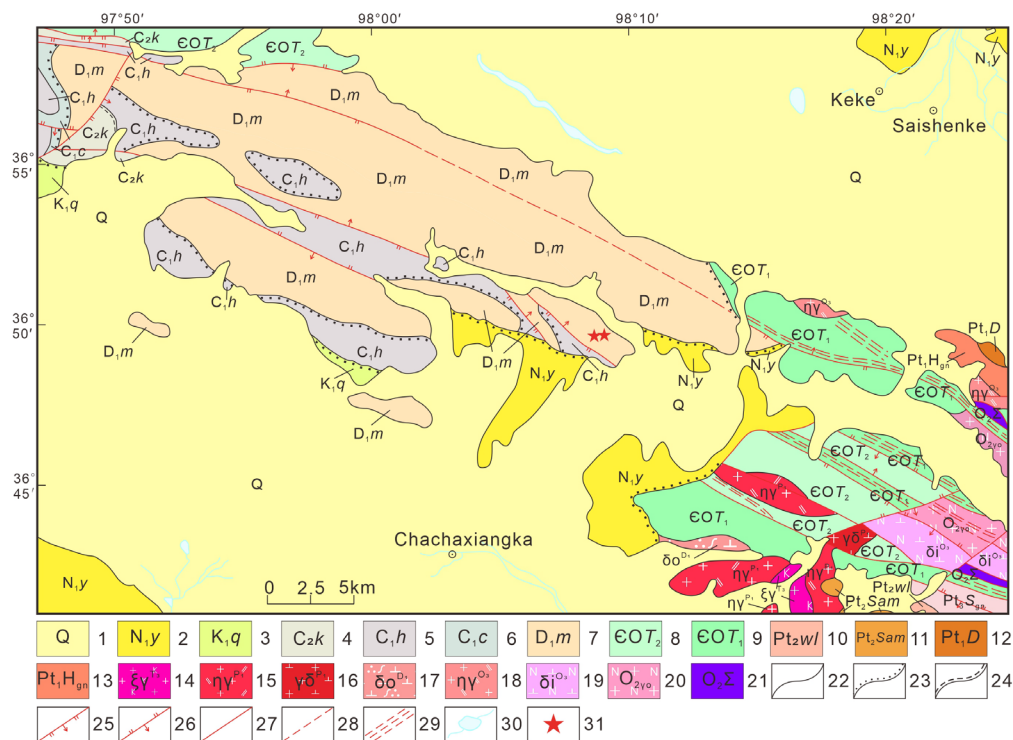


Figure 3. Simplified geological map of the Nankeke area, Wulan County, eastern segment of the NQ. 1—Q; 2—Miocene Youshashan Formation; 3—Lower Cretaceous Quanyagou Formation; 4—Upper Carboniferous Keluke Formation; 5—Lower Carboniferous Huaitoutala Formation; 6—Lower Carboniferous Chengqianggou Formation; 7—Early Devonian Maoniushan Formation; 8—Cambrian–Ordovician Tanjianshan Group metaclastic rocks; 9—Cambrian–Ordovician Tanjianshan Group metavolcanic rocks; 10—Mesoproterozoic Shaliuhe Group Wulongtan Formation; 11—Mesoproterozoic Shaliuhe Group plagioclase amphibolite formation; 12—Paleoproterozoic Dakendaban Group; 13—Paleoproterozoic Hudesheng gneiss; 14—Late Triassic syenogranite; 15—Early Permian monzogranite; 16—Early Permian granodiorite; 17—Early Devonian gneissic quartz diorite; 18—Late Ordovician monzogranite; 19—Late Ordovician tonalite; 20—Middle Ordovician plagioclase granite; 21—Middle Ordovician ultramafic rocks; 22—Geological boundary; 23—Angular unconformity; 24—Parallel unconformity; 25—Measured normal fault; 26—Measured reverse fault; 27—Measured fault with unknown nature; 28—Inferred fault; 29—Ductile shear zone; 30—Water system; 31—Sampling location.

Table 1. Paleoproterozoic–Mesozoic stratigraphic sequence for the Nankeke area in the NQ.

Time	Map Units	Rock Assemblages
Early Cretaceous	Quanyagou Formation	Siltstone, Sandstone, Conglomerate interlayered with mudstone
Permian–Jurassic		
Late Carboniferous	Keluke Formation	Limestone, Sandstone, Glutenite, Siltstone, Shale
Early Carboniferous	Huaitoutala Formation	Limestone, Quartz sandstone
	Chengqianggou Formation	Bioclastic limestone, Dolomite
Early Devonian	Maoniushan Formation	Sandstone, Siltstone, Glutenite, Basalt, Rhyolite, and Volcaniclastic rocks
Cambrian–Ordovician	Tanjianshan Group	Marble, Metabasaltic andesite, Andesite, Meta-crystalline tuff, Schist, and Siliceous rock
Neoproterozoic		
Mesoproterozoic	Shaliuhe Group	Amphibolite, Schist, Orthogneiss, and Paragneiss
Paleoproterozoic	Dakendaban Group	Amphibolite, Schist, Gneiss, Granulite, Quartzite, and Marble

Grey color: The geological units do not exist in this study area.

3. Petrography

In this paper, the bimodal volcanic rocks of the Maoniushan Formation are predominantly composed of rhyolitic crystal lithic tuff lava and minor basalts (Figure 4a–c), which have hardly undergone metamorphism and deformation. The basalts were interlayered between the felsic volcanic rocks. The samples were collected from the middle and upper sections of the Maoniushan Formation. Figure 3 shows the distribution location.

Basalts are grayish green in hand specimens and show a porphyritic texture (Figure 4c–e). They are composed of ~30% phenocrysts and ~70% matrix. The phenocrysts are mainly clinopyroxene, with a size of 1–3 mm and euhedral–subhedral columns, some of which have undergone chloritization and show cross interpenetration twinning (Figure 4e). The matrix grains have a size of <0.1 mm and consist mainly of fine columnar plagioclase microcrystals and other cryptocrystalline minerals, showing an interstitial texture, with varying degrees of secondary alteration. Rhyolitic crystal lithic tuff lava samples are grayish green–dull red in hand specimens, composed mainly of plagioclase (~5%), quartz (~20%), crystal fragments (~15%, including quartz, feldspar, and biotite), and rock debris (~60%, including rhyolite and rhyolitic tuff) (Figure 4f), indicating an intensive volcanic eruption event.

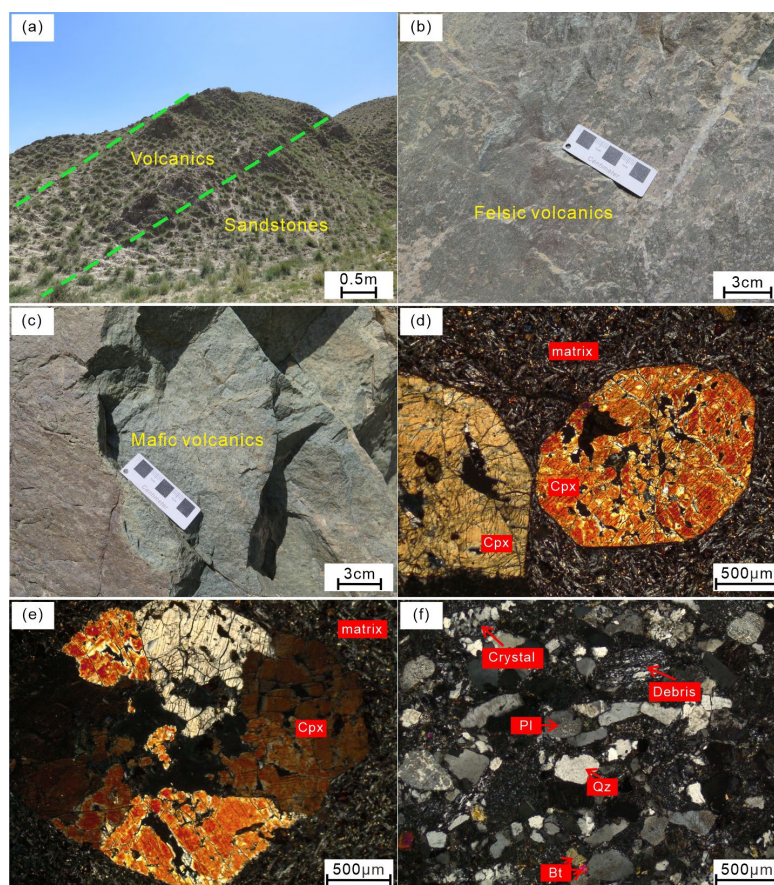


Figure 4. Maoniushan Formation volcanic rocks outcrops and photomicrographs. (a) Volcanic outcrop; (b) Felsic volcanic rocks outcrop; (c) Basalt outcrop; (d) Basalt micrograph and porphyritic structure; (e) Porphyritic structure and cross interpenetration twinning; (f) Microscopic features of felsic volcanic rocks. Minerals abbreviation: Cpx—clinopyroxene; Qz—quartz; Pl—plagioclase; Bt—biotite.

4. Analytical methods

4.1. Whole-Rock Geochemistry

Eleven samples were selected for major and trace element analysis at the Key Laboratory of Western China's Mineral Resources and Geological Engineering, Ministry of

Education, Chang'an University, Xi'an, China. The major elements were analyzed by the XRF method. To determine the oxide content, the samples were melted into glass disks, which were measured by an X-ray fluorescence spectrometer. Loss on ignition (LOI) was determined after igniting the sample power at 1000 °C for 1 h. Samples of trace and rare earth elements (REEs) were prepared by the high-pressure, closed, acidic decomposition method and then analyzed by Thermo-X7 Inductively Coupled Plasma Mass Spectrometry (ICP-MS). The analytical precision and accuracy were better than 10%. The analytical procedures were described by Tan et al. [81] and Chen et al. [82].

4.2. Zircon U-Pb Dating

Fresh samples were selected and crushed to 80–100 mesh using conventional methods. Zircons were separated by the flotation and electromagnetism techniques, and then handpicked using a binocular microscope. To reveal their internal structures, cathodoluminescence (CL) images were obtained on a scanning electron microscope equipped with a cathodoluminescence detector from Gaonianlinghang Technology Co., Ltd., Beijing, China. LA-ICP-MS zircon U-Pb experiments were performed at Kehui Testing Technology Co., Ltd., Beijing, China, and the State Key Laboratory of Continental Dynamics, Northwest University, Xi'an, China, respectively. Both diameters of the laser ablation spot beam were 30 µm, and the depth of the laser ablation samples was 20–40 µm. In the State Key Laboratory of Continental Dynamics, Northwest University, Xi'an, China, the analysis instruments were an Elan 6100DRC Type Quadrupole Perch Mass Spectrograph and a Geolas 200 M excimer laser ablation system (193 nm ArF laser). The detailed analytical procedures and instrument parameters are described by Li et al. [83] and Yuan et al. [84].

The international standard zircon 91,500 was used as an external standard for zircon age calculations. The artificial synthetic silicate glass NIST SRM610 was adopted as the external standard for element content analysis. ^{29}Si was used as the internal standard element. The data were analyzed using the ICPMS Datacal software (China University of Geosciences). Isoplot software (ver. 4.15) was used for the age calculation and concordia diagrams plot.

5. Analytical Results

5.1. Zircon Feature and U-Pb Dating

Basalts and felsic volcanic rocks (Samples No. DLH04-2 and DLH04-7) were collected for LA-ICP-MS U-Pb zircon dating to determine the crystallization ages of the volcanic rocks from the Maoniushan Formation in the eastern segment of the NQ. However, the U-Pb ages of the basalts were not obtained during the analysis, because a sufficient number of zircons were not obtained (number < 25) and the zircon grains were too small to be fully ablated by laser. Supplementary Table S1 lists the analytical data of the felsic volcanic rocks.

Twenty-five zircon grains were analyzed for U-Pb age determination for the felsic volcanic rocks of sample No. DLH04-2. The zircon grains are euhedral-subhedral, short, columnar, or equiaxial with clear boundaries, with crystal lengths of 100–200 µm and aspect ratios of 1:1–2:1. Most zircons show typical oscillatory zoning, indicative of magmatic zircon characteristics [85,86]. Some zircons have residual cores that may be inherited or trapped zircons (Figure 5a). Of the 25 analyzed zircons, 23 grains were analyzed on or near the U-Pb concordia lines (concordance > 90%) (Figure 6a,b). The results show that the Th and U contents range from 104 to 3064 (average of 695 ppm) and from 103 to 3345 (average of 1237) ppm, respectively (Figure 7a), and the Th/U ratios range from 0.21 to 2.03 (average of 0.61 > 0.4) (Figure 7b), also suggesting a magmatic origin [85–87]. In the U-Pb age spectrum (407–3468 Ma) (<1000 Ma, $^{206}\text{Pb}/^{238}\text{U}$ age; >1000 Ma, $^{207}\text{Pb}/^{206}\text{Pb}$ age) (Figure 6g), the youngest 7 zircon $^{206}\text{Pb}/^{238}\text{U}$ ages range from 407 Ma to 412 Ma, with a weighted mean $^{206}\text{Pb}/^{238}\text{U}$ age of 409.9 ± 3.9 Ma (MSWD = 0.067) (Figure 6c), which is interpreted as the crystallization age of the felsic volcanic rocks. However, the other older apparent ages represent the ancient magmatic events, in which an age of 3000–3500 Ma may indicate the existence of an Archean crystalline basement or continental core. An

age of ~2500 Ma suggests a strong tectonic–magmatic thermal event at the end of the Neoproterozoic. An ~1400 Ma single zircon age represents the existence of a Mesoproterozoic metamorphic terrane. An age of ~1000–900 Ma indicates the tectonic–magmatic thermal event from the late Mesoproterozoic to early Neoproterozoic, and it may be a response to the Neoproterozoic Rodinia supercontinent convergence event. An ~800 Ma zircon age may be a response to the breakup of the Rodinia supercontinent. An age of ~480–430 Ma may reflect the ocean–continent subduction magmatism in the Early Paleozoic.



Figure 5. Cathodoluminescence (CL) images and zircon U-Pb ages from the felsic volcanic rocks of the Maoniushan Formation.

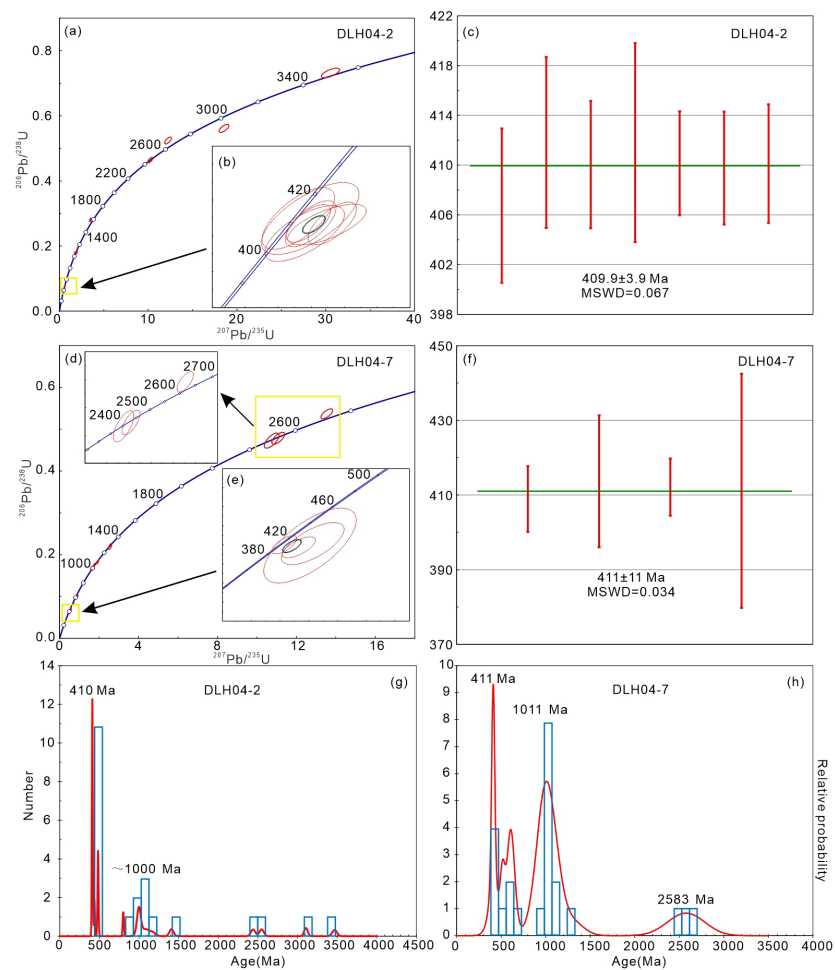


Figure 6. Zircon U-Pb age diagrams of felsic volcanic rocks in the Maoniushan Formation. (a,b) U-Pb concordia diagrams of DLH04-2 sample; (c) $^{206}\text{Pb}/^{238}\text{U}$ weighted mean ages of DLH04-2 sample; (d,e) U-Pb concordia diagrams of DLH04-7 sample; (f) $^{206}\text{Pb}/^{238}\text{U}$ weighted mean ages of DLH04-7 sample; (g) U-Pb age histogram of zircons from DLH04-2 sample; (h) U-Pb age histogram of zircons from DLH04-7 sample.

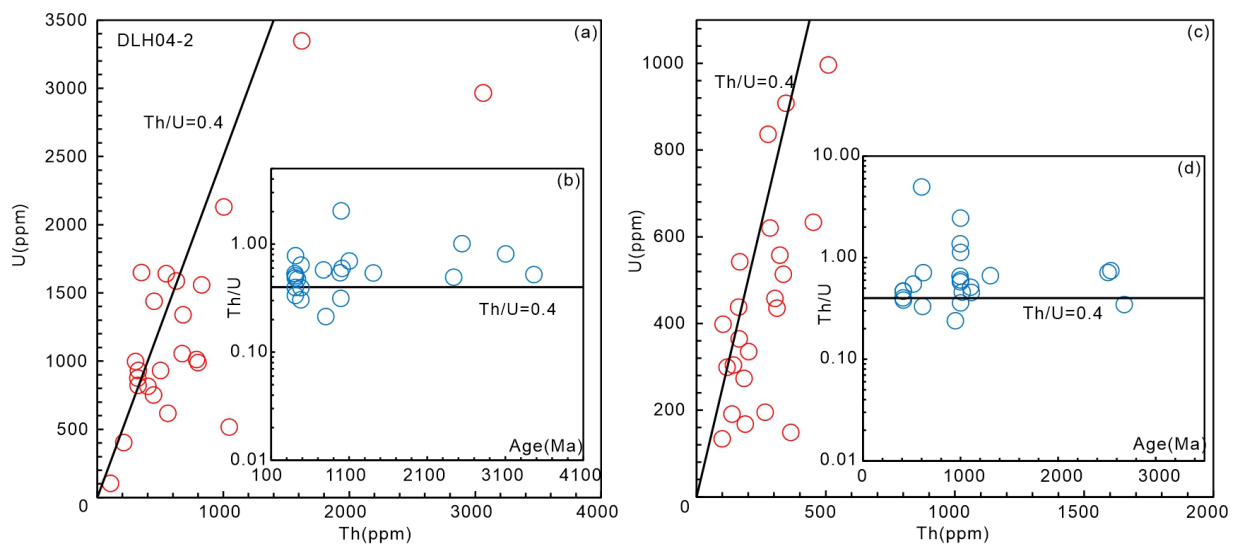


Figure 7. (a) Th vs. U content of zircon diagram of sample DLH04-2; (b) Age vs. Th/U of zircon diagram of sample DLH04-2; (c) Th vs. U content of zircon diagram of sample DLH04-7; (d) Age vs. Th/U of zircon diagram of sample DLH04-7 of the felsic volcanics in the Maoniushan Formation.

Twenty-five zircon grains were also selected for analysis for the felsic volcanic rocks of sample No. DLH04-7. The zircon features are similar to those of sample No. DLH04-2, with partially embayed boundaries (Figure 5b). The results show that the Th and U contents range from 100 to 1894 (average of 319 ppm) and from 134 to 998 (average of 455) ppm, respectively (Figure 7c). The Th/U ratios are highly variable and range from 0.24 to 4.96 (average value of 0.85 > 0.4) (Figure 7d), suggesting a magmatic origin [85–87]. In the U–Pb age spectrum (409–2677 Ma) (<1000 Ma, $^{206}\text{Pb}/^{238}\text{U}$ age; >1000 Ma, $^{207}\text{Pb}/^{206}\text{Pb}$ age; concordance > 90%), there is a major age peak at ~411 Ma and 2 minor age peaks at ~1011 Ma and ~2583 Ma (Figure 6h). The youngest 4 zircon $^{206}\text{Pb}/^{238}\text{U}$ ages range from 409 to 414 Ma, with a weighted mean $^{206}\text{Pb}/^{238}\text{U}$ age of 411 ± 11 Ma (MSWD = 0.034) (Figure 6d–f), representing the crystallization age of the felsic volcanic rocks. An age of ~2500 Ma indicates a strong tectonic–magmatic event at the end of the Neoproterozoic. An age of ~1300–900 Ma suggests a late Mesoproterozoic to early Neoproterozoic tectonic–magmatic event, possibly in response to the Rodinia supercontinent convergence event. An ~600 Ma zircon age may be a response to the break-up of the Rodinia supercontinent. An ~500 Ma single zircon age may have recorded the oceanic crustal subduction magmatism in the Early Paleozoic.

5.2. Geochemistry

Supplementary Table S2 presents the results of the whole-rock major and trace element analyses of the volcanic rocks from the Maoniushan Formation. The volcanic rock samples are mainly mafic volcanic rocks ($\text{SiO}_2 < 52$ wt.%) and felsic volcanic rocks ($\text{SiO}_2 > 63$ wt.%), showing the characteristics of bimodal volcanic rocks (Figure 8a).

5.2.1. Major Elements

The basalts are characterized by low contents of SiO_2 (48.92 wt.%–51.19 wt.%) and Na_2O (1.63 wt.%–2.30 wt.%) and relatively high contents of MgO (8.94 wt.%–9.99 wt.%), TiO_2 (1.05 wt.%–1.29 wt.%), K_2O (2.35 wt.%–4.17 wt.%), and $\text{K}_2\text{O}/\text{Na}_2\text{O}$ (1.04–2.56). On the SiO_2 vs. $\text{Na}_2\text{O} + \text{K}_2\text{O}$ diagram (Figure 8a) [88], the samples show the characteristics of alkaline–subalkaline basalts. On the SiO_2 vs. $\text{FeO}t/\text{MgO}$ and $\text{FeO}t-(\text{Na}_2\text{O} + \text{K}_2\text{O})-\text{MgO}$ diagrams (Figure 8b,c), these samples are further ascribed to the calc-alkaline basalt series [89]. The TiO_2 contents are in the range of continental flood basalts (=1.0 wt.%) and mid-ocean ridge basalts (=1.5 wt.%), which are different from the island arc basalts (<1.0 wt.%) [90], indicating that these samples are ascribed to continental basalts. In addition, the Mg# val-

ues of these samples range from 72.3 to 73.7, which are primitive magmas (>70), suggesting that these magmas have not undergone obvious fractional crystallization.

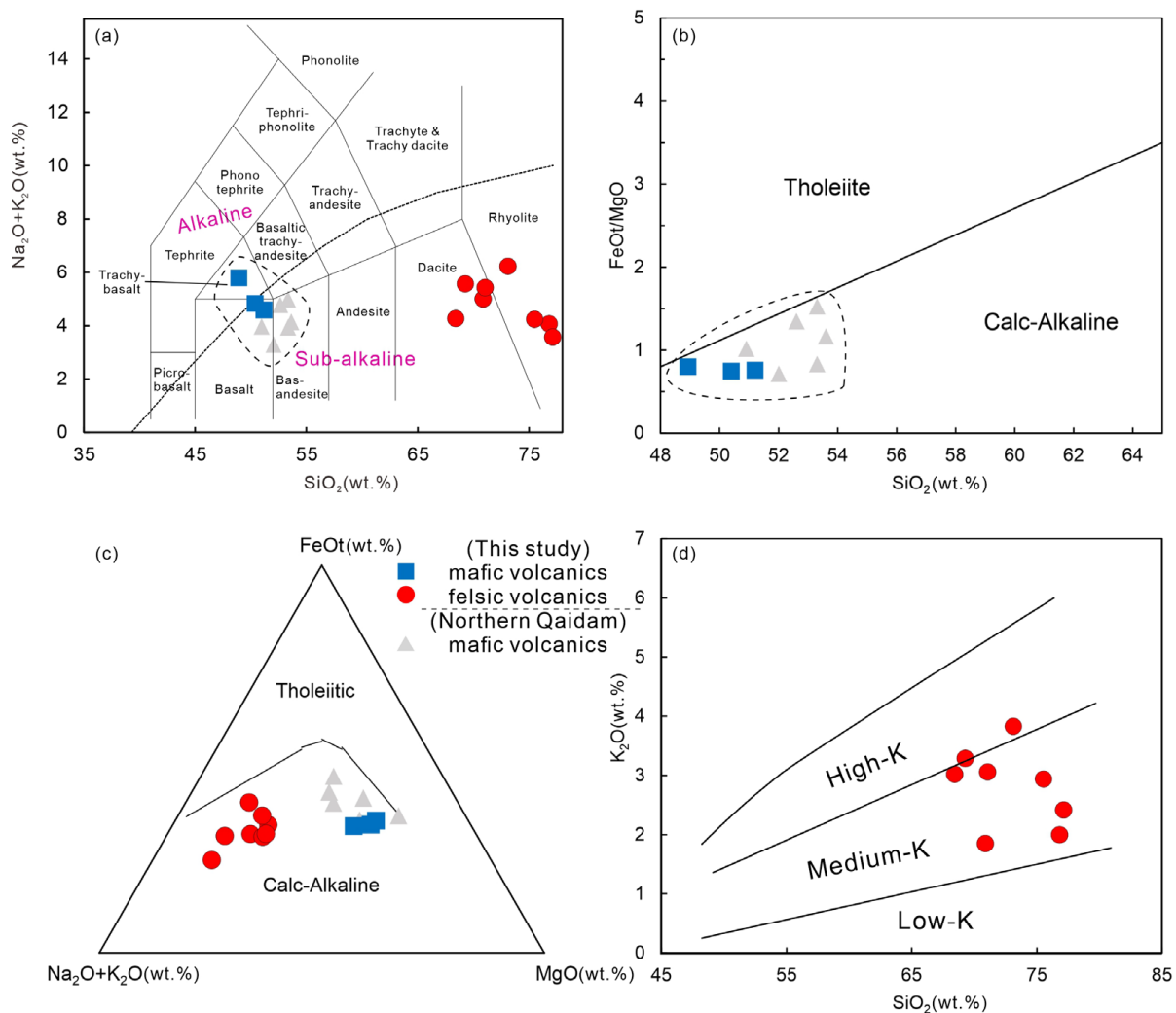


Figure 8. (a) SiO_2 vs. $\text{Na}_2\text{O} + \text{K}_2\text{O}$ diagram [88], (b) SiO_2 vs. FeOt/MgO diagram, (c) FeOt –($\text{Na}_2\text{O} + \text{K}_2\text{O}$)– MgO diagram, and (d) SiO_2 vs. K_2O diagram [89] for the volcanic rocks of the Maoniushan Formation. The data for mafic volcanics in the NQ are from Sun et al. [4].

The felsic volcanic rocks are silica-saturated, with high contents of SiO_2 (68.41 wt.%–77.12 wt.%) and MgO (1.29 wt.%–2.36 wt.%) and variable contents of $\text{Fe}_2\text{O}_3\text{T}$ (2.66 wt.%–5.02 wt.%), Na_2O (1.16 wt.%–3.16 wt.%), and K_2O (1.85 wt.%–3.83 wt.%). The A/CNK [molar $\text{Al}_2\text{O}_3 / (\text{CaO} + \text{K}_2\text{O} + \text{Na}_2\text{O})$] values of most samples range from 1.08 to 1.15 (except for two samples <1), indicating calc-alkaline peraluminous characteristics. The $\text{Mg}\#$ values range from 43.4 to 60.2 (average of 53.9), which are lower than the primitive magma ($\text{Mg}\# > 70$), suggesting that these magmas have undergone a relatively intense crystal fractionation [91]. On the SiO_2 vs. $\text{Na}_2\text{O} + \text{K}_2\text{O}$ diagram (Figure 8a) [88], these samples are in the calc-alkaline rhyolite range. On the FeOt –($\text{Na}_2\text{O} + \text{K}_2\text{O}$)– MgO and SiO_2 vs. K_2O diagrams (Figure 8c,d), the samples are further ascribed to the medium-K calc-alkaline series [89].

5.2.2. Trace Elements

The total REE contents of the basalts range from 331.91 to 518.33 ppm, with LREEs and HREEs ranging from 314.73 to 495.14 ppm and 17.19 to 23.20 ppm, respectively, showing relatively high LREE/HREE ratios (18.31–21.34). On the chondrite-normalized REE diagram (Figure 9a), they are characterized by LREEs enrichments and flat HREEs,

with $(La/Yb)_N$ values (34.87–42.80), $(La/Sm)_N$ values (4.38–4.56), and slightly negative Eu anomalies (0.82–0.86), resembling the reference line of OIBs.

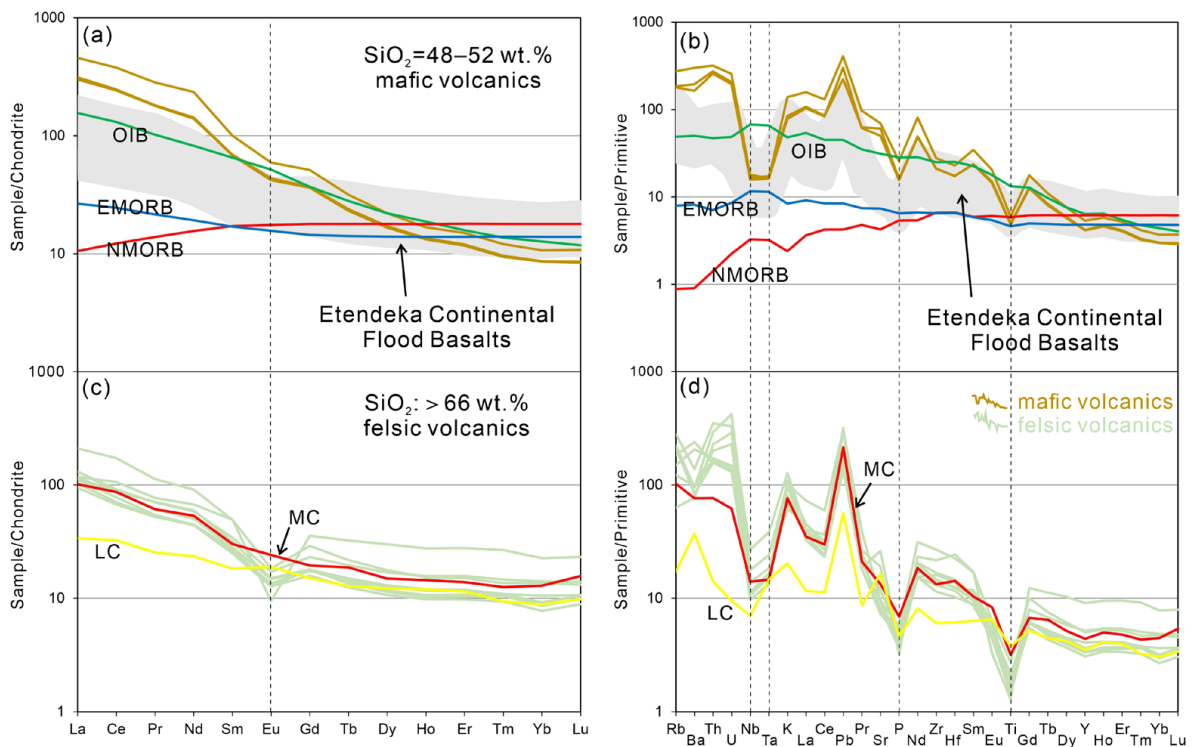


Figure 9. (a,c) Chondrite-normalized REE patterns; (b,d) Primitive-mantle normalized trace element spider diagrams for the Maoniushan Formation volcanics, eastern of the NQ. The chondrite data and the primitive mantle data for normalization are taken from Sun and McDonough [92]. The Low/Middle Crust (LC/MC) data are taken from Rudnick and Gao [93]. Oceanic island basalt (OIB), Enriched mid-ocean-ridge basalt (EMORB), and Normal mid-ocean-ridge basalt (NMORB) data are from Sun and McDonough [92]. Etendeka continental flood basalt data are from Ewart et al. [94,95].

On the primitive mantle-normalized trace element spider diagram (Figure 9b), the samples exhibit relative enrichments in large ion lithophile elements (LILEs; Rb, Th, and K) and depletions in high-field-strength elements (HFSEs; Nb, Ta, P, and Ti), which are similar to the continental flood basalt contaminated by the crust at Etendeka, Namibia [94,95], indicating that these may be related to asthenospheric mantle upwelling (plume) and continental extension.

The total REE contents of the felsic volcanic rock samples range from 106.83 to 234.71 ppm, with LREEs ranging from 314.73 to 495.14 ppm and HREEs between 10.40 and 27.41, indicating high LREE/HREE ratios (5.09–12.31). On the chondrite-normalized REE diagram (Figure 9c), they display enrichments in LREEs relative to HREEs, with $(La/Yb)_N$ values (5.20–15.43), $(La/Sm)_N$ values (2.38–4.35), and negative Eu anomalies (0.22–0.66). These characteristics are similar to those of the middle crust [93] and felsic volcanic rocks in the Amunike Mountain, Gouli, and Boluositai areas of the NQ [76–78]. On the primitive mantle-normalized trace element spider diagram (Figure 9d), the samples exhibit enrichments in LILEs (Rb, Th, U, K, and Pb) and depletions in HFSEs (Nb, Ta, P, and Ti). Overall, these features are similar to those of middle crustal rocks [93].

6. Discussion

6.1. Emplacement Ages of Bimodal Volcanic Rocks

Many studies have been conducted on the emplacement ages of volcanic rocks in the Maoniushan Formation. Zhang et al. [75] used LA-ICP-MS to obtain the zircon U–Pb ages of the rhyolitic ignimbrite of the Maoniushan Formation at the northern foot of the

Maoniushan area in the NQ, which are 396.5 ± 2.4 Ma and 395.8 ± 1.2 Ma, indicating that the volcanic rocks of the Maoniushan Formation were formed in the Early Devonian. The newly obtained zircon U–Pb ages of the felsic volcanic rocks in this study are 409.9 ± 3.9 Ma and 411 ± 11 Ma, indicating that the felsic volcanic rocks of the Maoniushan Formation at the southern foot of the Maoniushan area were formed in the Early Devonian. However, the U–Pb ages for the basalt were not obtained in this work, which requires further investigation. Based on field geological investigation, the felsic volcanics are widely distribution in this study area, which are spatially and temporally associated with the mafic volcanics. Combined with previous works on the Maoniushan Formation volcanic rocks in adjacent areas (e.g., East Kunlun), these indicate that the zircon U–Pb ages of the intermediate–felsic volcanic rocks of the Maoniushan Formation in the East Kunlun range from 423 to 399 Ma [73,74,77,96]. The bimodal volcanic rocks in the Boluositai area were also formed at 420–409 Ma in the Late Silurian to Early Devonian [78]. In contrast, the intermediate–felsic volcanic rocks in the NQ formed at 369–396 Ma, suggesting that these may have been formed in the Devonian and slightly later than those in the East Kunlun [43,75,76,97–100]. The youngest magmatic zircon age of 407.9 Ma is considered to be the depositional age of the sandstones of the Maoniushan Formation in Wulan County [101], indicating that the volcanic rocks of the Maoniushan Formation in Wulan County in the NQ were formed earlier than 407.9 Ma. Thus, in the study area, the ages of the volcanic rocks were determined to be ca. 410–409 Ma, indicating formation in the Early Devonian.

6.2. Petrogenesis

Based on field geological investigation, the outcrop volume of felsic volcanics is larger than that of mafic volcanics; they also have a close special and temporal relationship. The geochemical composition of the studied volcanic rocks shows a clear Daly gap between the mafic and felsic units. These all indicate a typical bimodal volcanic rock association. The possible influence of alteration on geochemistry must be ruled out prior to petrogenetic analysis. Zr is generally considered to be the most immobile element during metamorphism and alteration. The Zr element is compared to other elements to determine immobility [78,102,103]. REEs and HFSEs have a good linear relationship with Zr, suggesting that these elements were essentially immobile during metamorphism and alteration (Figure 10). In contrast, K, Ba, Na, and other fluid-mobile elements are mobile during metamorphism and alteration. Therefore, the immobile elements (e.g., REEs and HFSEs) are used to discuss the petrogenesis.

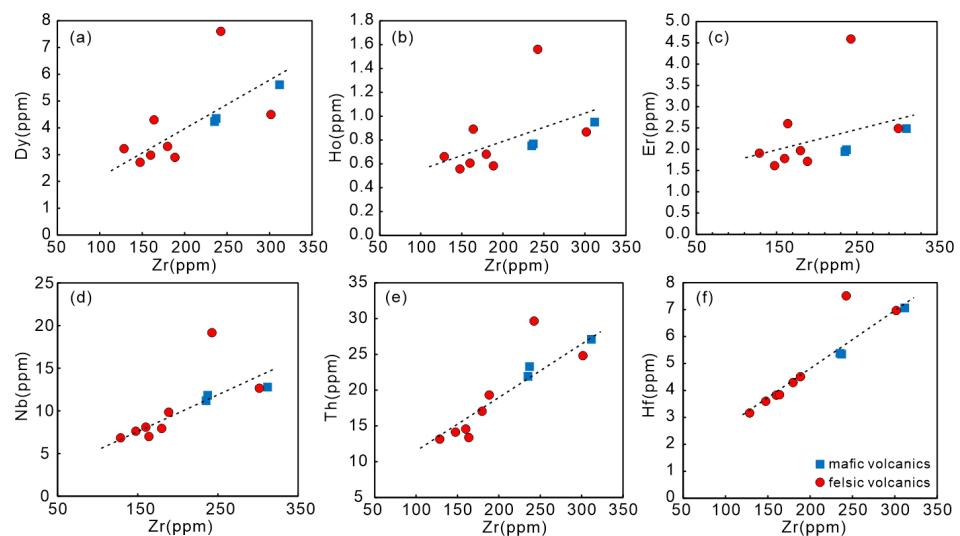


Figure 10. (a) Zr vs. Dy diagram, (b) Zr vs. Ho diagram, (c) Zr vs. Er diagram, (d) Zr vs. Nb diagram, (e) Zr vs. Th diagram, and (f) Zr vs. Hf diagram of bimodal volcanic rocks from the Maoniushan Formation.

(1) Magma source of basalts

Partial melting of mantle-derived magma has been recognized as the petrogenesis of basalts in bimodal volcanic rocks [78,104,105]. Nevertheless, the influence of crustal materials on the parental magma must be considered prior to the specific genetic analysis of basalts. The Mg#, Cr, and Ni values of basaltic rocks range from 72.3 to 73.7, 431.1 to 662.4, and 132.8 to 261.5 ppm, respectively, which are similar to those of primitive mantle melts ($Mg\# > 65$, Cr and Ni > 200 ppm) [88,106], probably suggesting that the basaltic magma did not undergo apparent fractional crystallization. The TiO_2 contents are between those of continental flood basalts (=1.0 wt.%) and mid-ocean ridge basalts (=1.5 wt.%), which are different from the island-arc basalts (<1.0 wt.%) [91,107–109], indicating the similarity with continental basalts. Furthermore, the REE patterns and trace element spider diagrams (Figure 9a,b) of the basalts resemble the characteristics of the OIB, suggesting a deep asthenospheric mantle source or plume [110]. However, the depletion of the “Nb–Ta–Ti” elements on the trace element spider diagram likely indicates a mantle source related to earlier subduction fluids. The high Zr contents (>200 ppm) and Zr/Yb values (>12) of the basalts and the Zr vs. Ti diagram (Figure 11a) show the characteristics of within-plate basalts (WPB), which are distinguished from island arc basalts (IAB), and exclude the possibility of subduction zone setting. In addition, incompatible trace elements are used to further consider the nature of the mantle source. The Zr/Nb values of the basalts range from 20 to 24, which are between the primitive mantle and the depleted mantle (PM = 14.8 and N-MORB = 30), suggesting an origin from the primitive mantle or depleted mantle source. The La/Nb values (6.25–8.48) and Ba/La values (16.17–19.27) are larger than PM (La/Nb = 0.94, Ba/La = 9.60) and N-MORB (La/Nb = 1.07, Ba/La = 4.00). The Th/La values ranging from 0.25 to 0.31 are similar to the continental crust (0.204), and the samples are plotted in the crustal contamination/lithospheric mantle region in the La/Nb vs. La/Ba diagram (Figure 12b) [111]. These characteristics provide further evidence that crustal materials may contaminate the asthenospheric mantle. In the Nb* vs. Ta* diagram (Figure 12c), those of the samples suggest that the continental crust material may originate from the upper crust. Additionally, the LREEs enrichments and HREEs depletions ($(La/Yb)_N = 34.87–42.80$, $(La/Sm)_N = 4.38–4.56$) of the basalt samples indicate that the mantle source probably contained some garnets. The Sm vs. Sm/Yb diagram (Figure 12a) further supported that the parental magmas might be derived from the garnet-bearing mantle source with low degrees (1%–5%) of partial melting [111].

Therefore, it can be concluded that the basalts are likely derived from low degrees (1%–5%) of partial melting of the asthenospheric mantle that was contaminated by small amounts of upper crustal material.

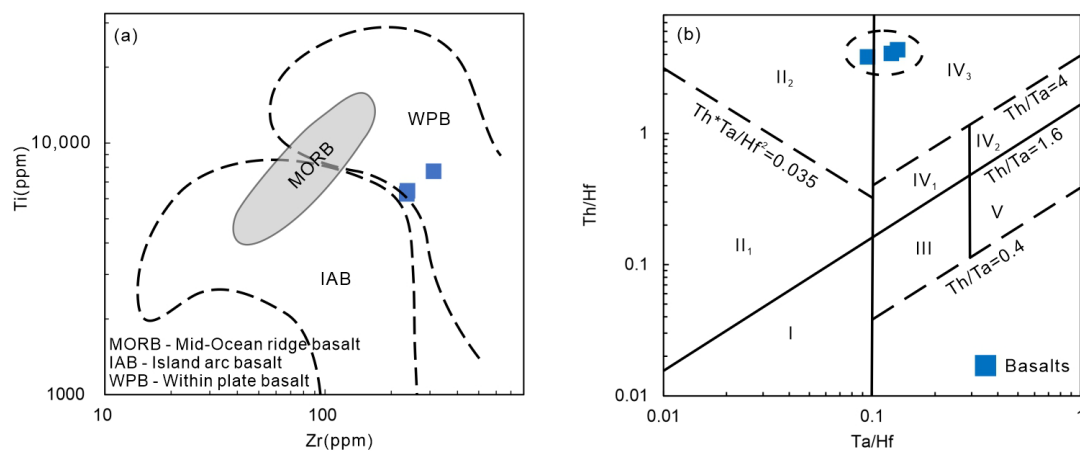


Figure 11. (a) Zr vs. Ti diagram and (b) Ta/Hf vs. Th/Hf diagram for basalts from the Maoniushan Formation. I—N-MORB; II₁—Ocean island basalts; II₂—Continental margin-arc basalts; III—Ocean intraplate basalts and E—MORB; IV₁—Intracontinental rift tholeiite basalts; IV₂—Intracontinental rift alkaline basalts; IV₃—Continental extension (or initial rift) basalts; V—Plume basalts.

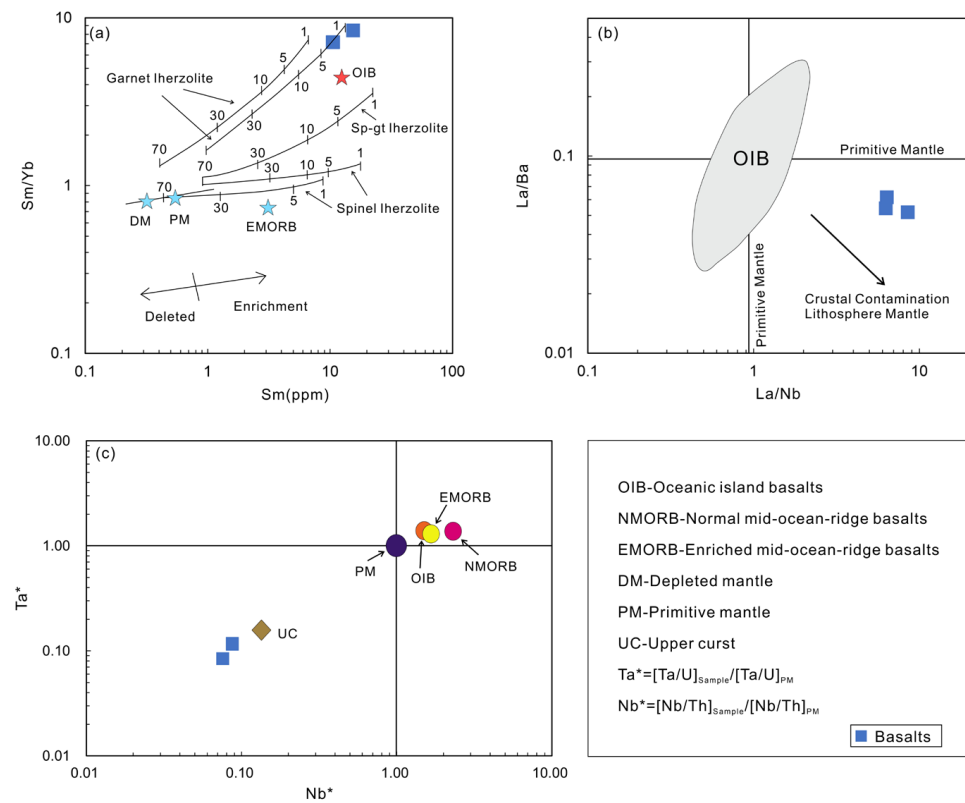


Figure 12. (a) Sm vs. Sm/Yb diagram [111], (b) La/Nb vs. La/Ba diagram [111], and (c) Nb* vs. Ta* diagram [112] for basalts from the Maoniushan Formation.

(2) Magma source of felsic volcanic rocks

As previously mentioned, the zircon U–Pb ages of the felsic volcanic rocks tested in this work have multiple peaks, which are mainly concentrated in the following six stages: ca. 3000–3500 Ma, ca. 2500 Ma, ca. 1300–900 Ma, ca. 600–800 Ma, ca. 500–430 Ma, and ca. 410 Ma. The data results show that most zircons have high Th/U ratios (>0.4) and obvious oscillatory zoning, suggesting a magmatic origin. Minor amounts of inherited zircons have residual cores with embayed boundaries, indicating that these zircons underwent metamorphism and hydrothermal alteration [86]. The ca. 3000–3500 Ma stage may indicate the existence of an Archean crystalline basement or continental core. The ca. 2500 Ma stage suggests a strong tectonic–magmatic thermal event at the end of the Neoproterozoic. The ca. 1300–900 Ma stage indicates the late Mesoproterozoic to early Neoproterozoic tectonic–magmatic thermal event and may be a response to the Neoproterozoic Rodinia supercontinent convergence event. The ca. 600–800 Ma stage may be a response to the breakup of the Rodinia supercontinent. The ca. 500–430 Ma stage may be a record of the Early Paleozoic subduction magmatism of the oceanic crust. The ca. 410 Ma stage represents the latest magmatic thermal event, which is interpreted as the crystallization age of the volcanic rocks. In general, the eastern segment of the NQ has experienced multiple tectonic–magmatic thermal events from the Archean to the early Late Paleozoic.

There are two possibilities for the genesis of felsic volcanic rocks in a bimodal volcanic suite, namely, (1) fractional crystallization of basaltic magmas [44,47,113] or (2) partial melting of mafic crust due to the underplating of mantle-derived basaltic magmas [46,114,115]. Based on geochemistry, there is a clear compositional gap between the mafic and felsic units, indicating different magma sources. Combined with the field geological investigation, the outcrop area/thickness of the felsic volcanic rocks is greater than that of the mafic rocks, suggesting that the relatively small volume of mafic magma could not produce the voluminous felsic rocks by fractional crystallization. Thus, it is argued that the partial melting of mafic crust generates the felsic volcanics. In the primitive mantle-normalized

trace element diagram (Figure 9d), the enrichments of LILEs (Rb, Th, U, K, and Pb) and the depletions of HFSEs (Nb, Ta, P, and Ti) resemble the middle continental crust [93]. The Rb/Sr values are mostly higher than 0.24 in this study area and adjacent areas (0.16–0.88, with an average value of 0.52; Gouli area: 1.10–2.28; NQ: 2.15–6.74) [76–78,116], which also shows the characteristics of the crust [117]. The high contents of Th (13.16–29.67) and Th/Ce values ($\text{Th/Ce} > 0.24$) and the Zr vs. Zr/Sm diagram (Figure 13a) further support the partial melting of the continental crust [118]. In the Nb/Y vs. Th/Y diagram (Figure 14b), all samples are plotted in the middle and lower crustal regions, suggesting an origin from the partial melting of the middle/lower crustal material. The $\text{K}_2\text{O} + \text{Na}_2\text{O} + \text{MgO} + \text{FeOT} + \text{TiO}_2$ vs. $(\text{K}_2\text{O} + \text{Na}_2\text{O})/(\text{MgO} + \text{FeOT} + \text{TiO}_2)$ diagram (Figure 14a) further proved these findings, as all samples are plotted in the amphibolite region, indicating that the felsic volcanic rocks are likely derived from a basaltic crustal material [119]. In addition, the characteristics of high SiO_2 content and depleted Eu, Ba, P, and Ti of the felsic volcanic rocks likely suggest that these rocks have undergone variable amounts of fractional crystallization (plagioclase, apatite, titanate).

Consequently, the felsic volcanic rocks of the Maoniushan Formation in this work area were formed by partial melting of amphibolite in the middle crust and underwent fractional crystallization to varying degrees.

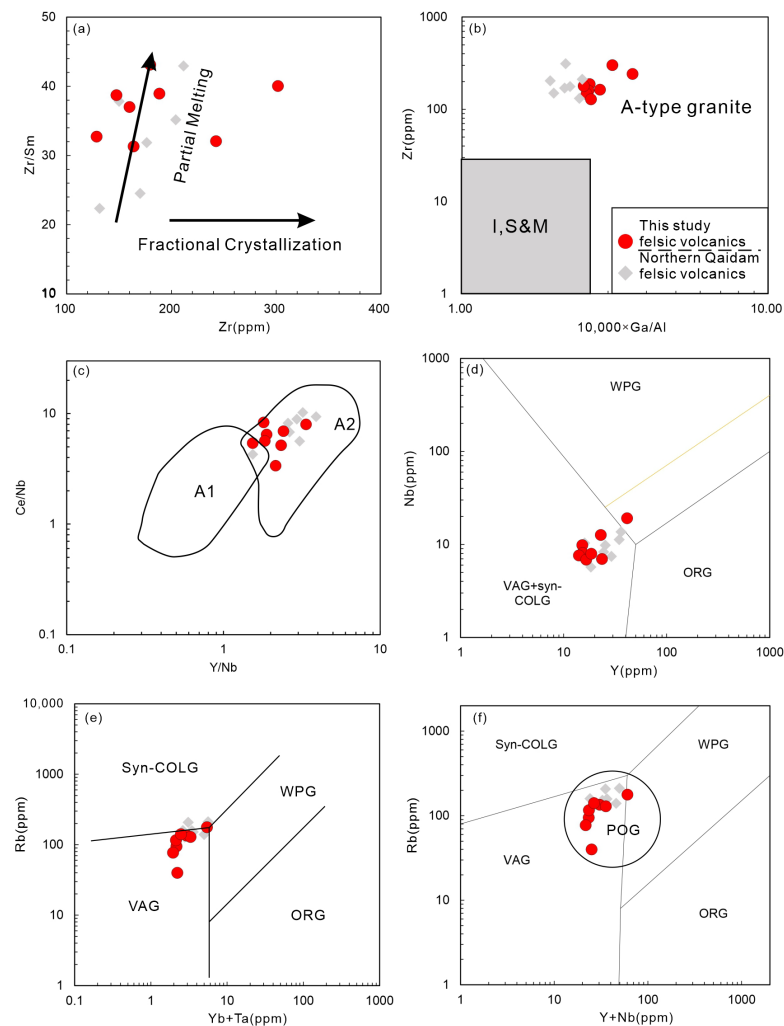


Figure 13. (a) Zr vs. Zr/Sm diagram, (b) $10,000 \times \text{Ga/Al}$ vs. Zr diagram [120], (c) Nb-Y-Zr diagram [121], (d) Y vs. Nb diagram, (e) $(\text{Yb} + \text{Ta})$ vs. Rb diagram, and (f) $(\text{Y} + \text{Nb})$ vs. Rb diagram [122] for felsic volcanic rocks from the Maoniushan Formation. The data for felsic volcanic rocks in the NQ are from Zhu et al. [123].

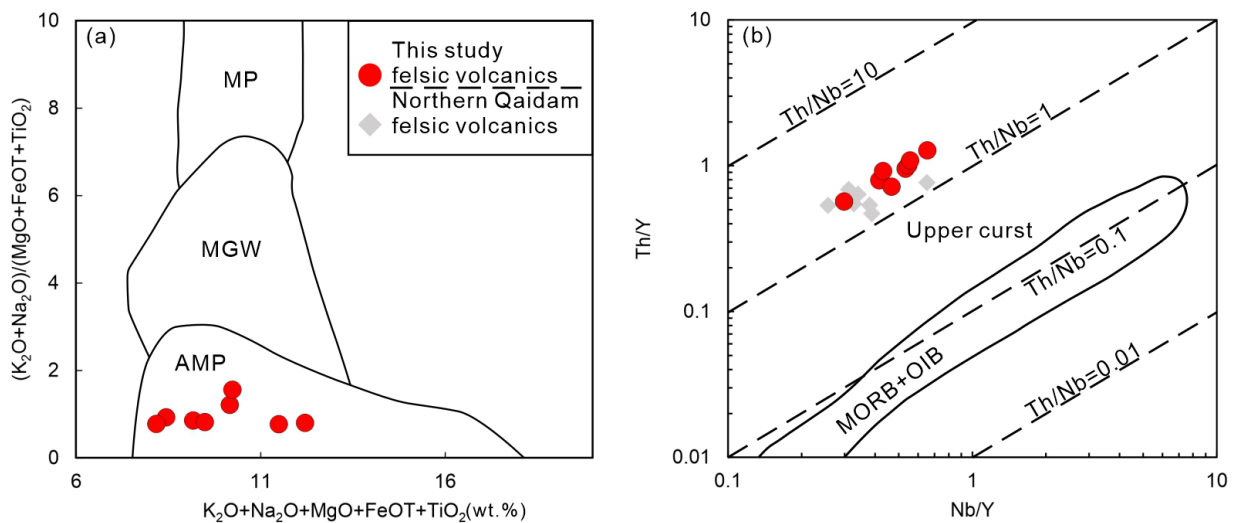


Figure 14. (a) $K_2O + Na_2O + MgO + FeOT + TiO_2$ vs. $(K_2O + Na_2O)/(MgO + FeOT + TiO_2)$ diagram [124] and (b) Nb/Y vs. Th/Y diagram [125] for felsic volcanic rocks from the Maoniushan Formation. The data for felsic volcanic rocks in the NQ are from Zhu et al. [123]. AMP-amphibolite; MGW- meta-greywackes; MP-metapelites.

6.3. Tectonic Setting and Magmatic Processes

6.3.1. Tectonic Setting

Generally, the bimodal volcanic suites are associated with extensional tectonic regimes and were generated in different tectonic settings, such as continental rift, a post-collisional setting, and back-arc basins [44–46,126–128]. The bimodal volcanic rocks are mainly composed of basalts and meta-alkaline felsic volcanic rocks in the post-collisional setting, which generally have A-type granite characteristics [89,129]. The Maoniushan Formation volcanic rocks mainly consist of calc-alkaline basalt and felsic rocks, with typical bimodal volcanic features, indicating an extensional tectonic setting. Geochemically, the Nb, Ta, and Ti elements of the basalts are strongly depleted due to crustal contamination, which is generally interpreted as an arc-related setting. The basaltic units have high contents of Zr (>200 ppm) and the Zr/Yb ratio (>12), and in the Zr vs. Ti diagram (Figure 11a), suggesting the characteristics of continental intraplate basalts [130]. The high LREE/HREE (18.31–21.34) and TiO₂ values (1.05 wt.%–1.29 wt.%) and relative enrichments of LILEs and LREEs show the nature between CFB and OIB, indicating the affinity of the intraplate extension setting [109]. In the Ta/Hf vs. Th/Hf diagram (Figure 11b), these samples are plotted in the continental margin arc and continental extension (or initial rift) basalts areas, further proving the intraplate extension setting [131]. Furthermore, in the $10,000 \times Ga/Al$ vs. Zr diagram, all felsic volcanic samples are plotted in the A-type granite range (Figure 13b), further suggesting a post-collisional extensional setting. In the Y/Nb vs. Ce/Nb diagram (Figure 13c), these rocks are further ascribed to A-2 type granite [121], which is a response to the post-collisional extensional setting. The felsic volcanic samples are mostly plotted on or near the intersection of volcanic arc granite (VAG) and collisional granite (Syn-COLG), and within-plate granite (WPG) in the Y vs. Nb (Figure 13d), (Yb + Ta) vs. Rb (Figure 13e), and (Y + Nb) vs. Rb (Figure 13f) diagrams, which are described as the post-collisional granite [122]. Regionally, a suit of Late Silurian to Late Devonian molasses deposits was generally distributed in the NQ, suggesting the rapid uplift of the upper crust and regional extension. It is summarized that the Nankeke area in Wulan County of the NQ was in the post-collisional extensional setting of the Early Devonian.

The large number of Early Paleozoic rock records related to ocean evolution in the NQ and adjacent areas supports the existence of the ancient Qaidam Ocean between the Qaidam Block and the Quanji–Qilian Block in the Early Paleozoic [4,10,21–23,59,132,133]. Regionally, as a branch of the Proto-Tethys Ocean, the duration of the ancient Qaidam

Ocean was similar to that of the Central Kunlun Ocean, the North Qilian Ocean, and the Wushan–Shangdan Ocean in the Central Orogenic Belt, China [20,43,78,80,134–145]. Moreover, as an independent subduction/collision complex belt, most scholars have suggested that the NQ experienced a single northward ocean–continent subduction in the Early Paleozoic [4,5,7,133,146–148]. The ophiolitic mélanges near the Shaliuhe, Lvliangshan, and Taipinggou areas recorded the deep subduction of the oceanic crust with a formation age of 535–496 Ma [23,70–72]. The subduction-related rock assemblages and the typical island arc volcanic rocks of the Tanjianshan Group (514–460 Ma) indicate that the oceanic crust was subducted before ca. 460 Ma [5,9,10,17,21,22,133,138,149–155]. Following the subduction processes, the ancient Qaidam Ocean finally closed in the Middle to Late Ordovician (ca. 460–450 Ma), dragging the Qaidam Block into continental deep subduction, which implies that the NQ evolved into a continental subduction/collision orogeny stage [15,24–28]. The eclogites and granites in the North Qaidam UHP/HP Metamorphic Belt recorded the continental deep subduction, which constrained the timing of the continental subduction/collision at 420–460 Ma [43]. The Maoniushan Formation molasses have been widely accepted to record the evolution process from large-scale rapid uplift to the regional extension, with voluminous magmatism. The identification of bimodal volcanic rocks at 410–409 Ma in this study area represents the tectonic transition from compressional to extensional regimes and the evolution into the post-collisional extensional stage (Figure 15).

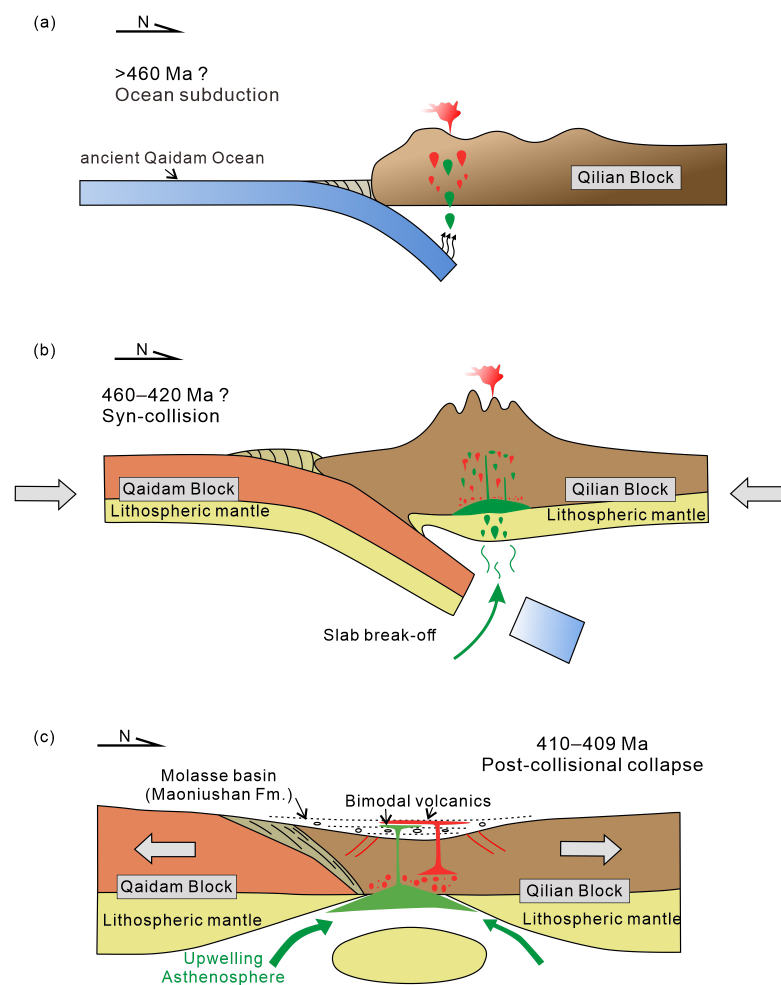


Figure 15. Schematic diagrams showing the tectonic evolution of NQ. (a) Oceanic subduction beneath the Qilian Block, (b) Qaidam Block collided with Qilian Block, and (c) the bimodal volcanic magmatism and delamination modal of the Maoniushan Formation in the post-collisional extensive stage [156–158].

The large number of Devonian magmatism related to the post-collision extensional regime marks the end of the Proto-Tethyan tectonic cycle and the beginning of the Paleo-Tethyan tectonic cycle. However, the existence of the Late Paleozoic to Early Mesozoic Paleo-Tethyan Ocean in the NQ is still a controversial scientific problem, thus leading to different viewpoints on the genesis of the Late Permian to Middle Triassic arc-related magmatic rocks. Some scholars have suggested that these rocks, including the Chahanuo gabbro, granite, and granodiorite (241–256 Ma); Chahanhe granodiorite and diorite (243 ± 1 Ma and 245 ± 0.7 Ma, respectively); and Guokeshan quartz diorite and mafic microgranular enclaves (MMEs) (ca. 247 Ma), are interpreted as a remote response to the northward subduction of the ancient Tethys Ocean (A'nyemaqen–Buqingshan Ocean). The NQ experienced intracontinental rifting only during the Late Hercynian to Indosinian and did not form an ocean basin [39–43]. Nevertheless, most scholars have suggested the existence of the Zongwulong Ocean (a branch of the Paleo-Tethys Ocean) in the NQ during the Late Hercynian to Indosinian [32–38]. The outcrop of Devonian strata in the Zongwulong Tectonic Belt and the Devonian diabase dyke ($^{40}\text{Ar}/^{39}\text{Ar}$ age, 393.5 ± 3.0 Ma) in the Lalongwa in the Kuhai–Saishitang area [159] indicate that the initial rifting of the Zongwulong Tectonic Belt occurred in the Early Devonian and then evolved into the continental rift stage, which is consistent with the tectonic evolution of the Maoniushan in the Wulan area. The Late Carboniferous ophiolitic mélangé of the Guokeshan Formation in Tianjun Nanshan (Rb–Sr isochron ages, 318 ± 3 Ma and 331.31 ± 88 Ma) represents the formation of the Zongwulong Ocean [32,35]. The Late Permian–Middle Triassic arc-related magmatic rocks are a response to the southward subduction of the Zongwulong Ocean [36–38,97]. The sedimentary sequence of the Wulonghe Group records the progressive deepening trend from shallow to deep water, further supporting the existence of the Zongwulong Ocean [80,97,160]. The combination of the contemporaneous A'nyemaqen–Buqingshan Ocean and Kuhai–Saishitang oceanic–continental transition-type aulacogen and the related Late Paleozoic residual ocean basins suggested the tectonic framework of the Late Hercynian–Indosinian Paleo-Tethys Archipelago Ocean in the northern margin of the Tibetan Plateau [33–35,159,161–164].

In summary, with the continuous subduction of the ancient Qaidam oceanic crust, the Qaidam Block was dragged to begin deep subduction in the Middle and Late Ordovician, representing the closure of the Proto-Tethys Ocean, and evolved to the continental subduction/collision orogeny stage. After large-scale collisional orogeny, the NQ evolved to the post-collisional extensional stage in the Early Devonian, marking the tectonic transition from compressional to extensional regimes and opening the Paleo-Tethys tectonic cycle. Finally, the formation of the Zongwulong Ocean in the Late Carboniferous suggests the tectonic framework of the Late Hercynian–Indosinian Paleo-Tethys Archipelago Ocean at the northern margin of the Tibetan Plateau.

6.3.2. Magmatic Processes

Generally, the collisional orogeny and compression between different blocks results in thickening of the lithosphere [165]. In the thickening processes, the lower mafic crust rocks were converted into eclogites with higher density by metamorphism, resulting in the delamination of the lithosphere into the asthenospheric mantle due to gravitational instability, further causing the upwelling of high-temperature and low-density asthenospheric materials, with a large amount of magmatism [52–54,156–158,165–168]. The Early Devonian Maoniushan Formation bimodal volcanic rocks were identified in the NQ, indicating that the lithospheric delamination evolved in the post-collisional extensional stage. For the study area, the delamination events resulted in upwelling and decompression melting of the asthenospheric mantle, thus generating the calc-alkaline basalts, with the contamination of minor crustal materials. The ascending asthenospheric mantle/mafic melt could further intrude the lithosphere and supply additional heat to the crust, resulting in partial melting of the crust and producing the contemporaneous high-temperature felsic volcanic rocks. Based on the equation of Watson and Harrison [169], the estimated

zircon saturation temperatures (T_{Zr} (°C)) of the felsic volcanic rocks are between 752 °C and 890 °C, with an average of 830 °C, suggesting that these rocks were formed in a high-temperature setting and are consistent with the A-type granite, which could be a response to the thermal input of the underplating of basaltic magma and/or upwelling asthenospheric mantle by post-collisional delamination [78,170,171]. The previous analysis and geochemical characteristics suggest that the felsic volcanic rocks in this work may have been directly produced by the partial melting of crustal materials, without the interaction of mantle melt.

Accordingly, the model of the delamination and asthenospheric upwelling in the post-collision stage can well account for the formation of bimodal volcanic rocks of the Maoniushan Formation in the eastern segment of the NQ (Figure 15c) and explain the mechanism of rapid crustal uplift and the molasses deposition in this region.

7. Conclusions

1. The bimodal volcanic suite of the Maoniushan Formation in the NQ is composed of rhyolitic crystal lithic tuff lava and minor basalts. The LA-ICP-MS zircon U-Pb ages indicate that these volcanic rocks formed in the Early Devonian (ca. 410–409 Ma).
2. The geochemical features indicate that the basalts were produced by the low degree (1%–5%) of partial melting of the garnet mantle source, with minor contamination by the upper crustal materials. The felsic volcanic rocks are the products of the partial melting of basaltic crustal materials, without mantle melt interaction.
3. The Early Devonian bimodal volcanic rocks in the eastern segment of the NQ formed in a post-collisional extensional setting related to delamination and asthenospheric mantle upwelling.
4. Based on the formation ages, geochemistry, and rock assemblages, the Proto-Tethys Ocean had been closed during the Middle and Late Ordovician and evolved in a continental subduction/collision orogeny stage. In the Early Devonian, it evolved into the post-collisional extensional stage and began the rapid crustal uplift and the deposition of the Maoniushan Formation molasses, marking the tectonic transition from the compressional to extensional regimes. Finally, the Zongwulong Ocean was formed in the Late Carboniferous, representing the tectonic framework of the Paleo-Tethys Archipelago Ocean.

Supplementary Materials: The following supporting information can be downloaded at: <https://www.mdpi.com/article/10.3390/min13040532/s1>, Table S1. Zircon U-Pb isotopic analysis data of Bimodal volcanic rocks of Maoniushan Formation from Nankeke area in North Qaidam Belt; Table S2. Geochemical data of major (wt.%), trace (ppm) and rare earth elements of bimodal volcanic rocks of Maoniushan Formation from Nankeke area in North Qaidam Belt.

Author Contributions: Conceptualization, M.W. and X.P.; methodology, M.W. and X.P.; software, H.L. and M.W.; validation, M.W. and X.P.; formal analysis, M.W., Z.L., X.P. and R.L.; investigation, M.W., Z.L., H.L., X.P., L.X., L.P. and C.L.; resources, R.L., Z.L. and X.P.; data curation, M.W. and X.P.; writing—original draft preparation, M.W. and X.P.; writing—review and editing, M.W., R.L. and X.P.; visualization, M.W.; supervision, Z.L., R.L. and X.P.; project administration, Z.L., X.P. and R.L.; funding acquisition, Z.L., X.P. and R.L. All authors have read and agreed to the published version of the manuscript.

Funding: This research was funded by the National Natural Science Foundation of China (Grant Nos. 42172236, 41502191, 41872233, 41872235, 41472191), National Science Foundation of Shaanxi Province of China (Grant Nos. 2020JM-229), China Scholarship Council (Grant Nos. 201906565008), the Fundamental Research Funds for the Central Universities, CHD (Grant Nos. 300102279204), and the Youth Innovation Team of Shaanxi Universities.

Data Availability Statement: The original contributions presented in the study are included in the article/Supplementary Materials.

Acknowledgments: We would like to thank the Key Laboratory of Western China's Mineral Resources and Geological Engineering, Ministry of Education, Chang'an University, Xi'an, China, and the State Key Laboratory of Continental Dynamics, Northwest University, Xi'an, China, for support and assistance on zircon U-Pb and major and trace elements analysis. The authors would like to thank Enago (www.enago.cn (accessed on 21 February 2023)) for the English language review. The authors are grateful for the contributions from S.J. and X.W., which improved the completion of this manuscript. The authors are grateful for the critical comments from the chief editor and the anonymous reviewers, which profoundly enhanced the quality of this manuscript.

Conflicts of Interest: The authors declare no conflict of interest.

References

1. Xin, H.T.; Wang, H.C.; Zhou, S.J. Geological Events and Tectonic Evolution of the North Margin of the Qaidam Basin. *Geol. Surv. Surv. Res.* **2006**, *29*, 311–320.
2. Zhang, J.X.; Yu, S.Y.; Li, Y.S.; Yu, X.X.; Lin, Y.H.; Mao, X.H. Subduction, accretion and closure of Proto-Tethyan Ocean: Early Paleozoic accretion/collision orogeny in the Altun-Qilian-North Qaidam orogenic system. *Acta Petrol. Sin.* **2015**, *31*, 3531–3554.
3. Ren, Y.F. Mesoproterozoic to Early Paleozoic Tectonic Evolution of the North Qaidam Orogenic Belt. Ph.D. Thesis, Northwest University, Xi'an, China, 2017.
4. Sun, G.C. Reworking and Recycling of the Subducted Crustal Materials: Geochemical Evidence from Paleozoic Magmatic Rocks in the North Qaidam Orogen. Ph.D. Thesis, University of Science and Technology of China, Hefei, China, 2020.
5. Zhu, X.H. Magmatic Response to the Early Paleozoic Tectonic Transition in the South Qilian and North Qaidam and its Constraints on Orogenic Process. Ph.D. Thesis, Northwest University, Xi'an, China, 2021.
6. Xia, L.Q.; Xia, Z.C.; Xu, X.Y. Early Paleozoic oceanic ridge-ocean island and back-arc basin volcanism in the North Qilian Mountains. *Acta Geol. Sin.* **1998**, *4*, 301–312.
7. Xu, Z.Q.; Yang, J.S.; Li, H.B.; Yao, J.X. The Early Palaeozoic Terrene Framework and the Formation of the High-Pressure (HP) and Ultra-High Pressure (UHP) Metamorphic Belts at the Central Orogenic Belt (COB). *Acta Geol. Sin.* **2006**, *80*, 179–1806.
8. Xu, Z.Q.; Yang, J.S.; Li, W.C.; Li, H.Q.; Cai, Z.H.; Yan, Z.; Ma, C.Q. Pako-Tethys system and accretionary orogen in the Tibet Plateau. *Acta Petrol. Sin.* **2013**, *29*, 1847–1860.
9. Wu, C.L.; Gao, Y.H.; Wu, S.P.; Chen, Q.L.; Wooden, J.L.; Mazadab, F.K.; Mattinson, C. Zircon SHRIMP U-Pb dating of granites from the Da Qaidam area in the north margin of Qaidam basin, NW China. *Acta Petrol. Sin.* **2007**, *23*, 1861–1875.
10. Wu, C.L.; Gao, Y.H.; Wu, S.P.; Chen, Q.L. Zircon SHRIMP U-Pb dating and Geochemistry of granites in the western segment of the North Qaidam. *Sci. China Ser. D Earth Sci.* **2008**, *38*, 930–949.
11. Ren, J.H. A Study on Tectonic Evolution during the Period of Nanhua to Devonian at the North and South of Qaidam Basin. Ph.D. Thesis, Northwest University, Xi'an, China, 2010.
12. Song, S.G.; Niu, Y.L.; Su, L.; Wei, C.J.; Zhang, L.F. Adakitic (tonalitic-trondhjemitic) magmas resulting from eclogite decompression and dehydration melting during exhumation in response to continental collision. *Geochim. Cosmochim. Acta* **2014**, *130*, 42–62. [[CrossRef](#)]
13. Song, S.G.; Niu, Y.L.; Su, L.; Zhang, C.; Zhang, L.F. Continental orogenesis from ocean subduction, continent collision/subduction, to orogen collapse, and orogen recycling: The example of the North Qaidam UHPM belt, NW China. *Earth-Sci. Rev.* **2014**, *129*, 59–84. [[CrossRef](#)]
14. Zhang, J.X.; Yu, S.Y.; Mattinson, C.G. Early Paleozoic polyphase metamorphism in northern Tibet, China. *Gondwana Res.* **2017**, *41*, 267–289. [[CrossRef](#)]
15. Zhang, L.; Chen, R.X.; Zheng, Y.F.; Hu, Z.C.; Xu, L.J. Whole-rock and zircon geochemical distinction between oceanic- and continental-type eclogites in the North Qaidam orogen, northern Tibet. *Gondwana Res.* **2017**, *44*, 67–88. [[CrossRef](#)]
16. Gao, X.Y.; Yu, S.Y.; Li, S.Z.; Santosh, M.; Liu, Y.J.; Jiang, X.Z.; Peng, Y.B.; Zhao, S.W.; Lv, P. Syn-collisional I-type granitoids linked to lateral lithospheric heterogeneity: A case study from the North Qaidam orogen, NW China. *J. Asian Earth Sci.* **2022**, *237*, 105363. [[CrossRef](#)]
17. Wang, B.Z.; Fu, C.L.; Pan, T.; Li, Q.; Lu, Y.Z.; Jin, T.T. Early Paleozoic magmatism and tectonic evolution in Saishiteng area, the North Qaidam. *Acta Petrol. Sin.* **2022**, *38*, 2723–2742.
18. Sengör, A.M.C.; Natal'in, B.A. Paleotectonic of Asia: Fragments of a synthesis. In *The Tectonic Evolution of Asia*; Yin, A., Harrison, M., Eds.; Cambridge University Press: Cambridge, UK, 1996; pp. 486–640.
19. Pan, G.T.; Wang, L.Q.; Li, R.S.; Yuan, S.H.; Ji, W.H.; Yin, F.G.; Zhang, W.P.; Wang, B.D. Tectonic evolution of the Qinghai-Tibet Plateau. *J. Asian Earth Sci.* **2012**, *53*, 3–14. [[CrossRef](#)]
20. Pan, Y.S.; Zhou, W.M.; Xu, R.H.; Wang, D.A.; Zhang, Y.Q.; Xie, Y.W.; Chen, T.E.; Luo, H. Geological characteristics and evolution of Kunlun Mountains in the Early Paleozoic. *Sci. China Ser. D* **1996**, *26*, 302–307.
21. Shi, R.D.; Yang, J.S.; Wu, C.L.; Tsuyoshi, I.; Takafumi, H. Island arc volcanic rocks in the north Qaidam UHP belt, northern Tibet plateau: Evidence for ocean-continent subduction preceding continent-continent subduction. *J. Asian Earth Sci.* **2006**, *28*, 151–159.
22. Zhu, X.H.; Chen, D.L.; Liu, L.; Li, D. Zircon LA-ICP-MS U-Pb dating of the Wanggaxiu gabbro complex in the Dulan area, northern margin of Qaidam Basin, China and its geological significance. *Geol. Bull. China* **2010**, *29*, 227–236.

23. Zhu, X.H.; Chen, D.L.; Liu, L.; Zhao, J.; Zhang, L. Geochronology, geochemistry and significance of the Early Paleozoic back-arc type ophiolite in Lvliangshan area, North Qaidam. *Acta Petrol. Sin.* **2014**, *30*, 822–834.
24. Chen, D.L.; Sun, Y.; Liu, L. Zircon U-Pb dating of paragneiss interbed in the UHP eclogite from Yematan area, the North Qaidam UHP terrane, NW China. *Acta Petrol. Sin.* **2008**, *24*, 1059–1067.
25. Chen, D.L.; Liu, L.; Sun, Y.; Sun, W.D.; Zhu, X.H.; Liu, X.M.; Guo, C.L. Felsic veins within UHP eclogite at Xitieshan in North Qaidam, NW China: Partial melting during exhumation. *Lithos* **2012**, *136–139*, 187–200. [[CrossRef](#)]
26. Yu, S.Y.; Zhang, J.X.; Sun, D.Y.; Li, Y.S.; Gong, J.H. Anatexis of ultrahigh-pressure eclogite during exhumation in the North Qaidam ultrahigh-pressure terrane: Constraints from petrology, zircon U-Pb dating, and geochemistry. *Geol. Soc. Am. Bull.* **2015**, *127*, 1290–1312.
27. Yu, S.Y.; Zhang, J.X.; Sun, D.Y.; del Real, P.G.; Li, Y.S.; Zhao, X.L.; Hou, K.J. Petrology, geochemistry, zircon U-Pb dating and Lu-Hf isotope of granitic leucosomes within felsic gneiss from the North Qaidam UHP terrane: Constraints on the timing and nature of partial melting. *Lithos* **2015**, *218–219*, 1–21.
28. Zhang, L.; Chen, R.X.; Zheng, Y.F.; Li, W.C.; Hu, Z.; Yang, Y.H.; Tang, H.L. The tectonic transition from oceanic subduction to continental subduction: Zirconological constraints from two types of eclogites in the North Qaidam orogen, northern Tibet. *Lithos* **2016**, *244*, 122–139. [[CrossRef](#)]
29. Xu, Z.Q.; Yang, J.S.; Li, H.B.; Zhang, J.X.; Wu, C.L. *Orogenic Plateau*; Geological Press: Beijing, China, 2007; pp. 191–194.
30. Li, R.S.; Ji, W.H.; Zhao, Z.M.; Chen, S.J.; Meng, Y.; Yu, P.S.; Pan, X.P. Progress in the study of the Early Paleozoic Kunlun orogenic belt. *Geol. Bull. China* **2007**, *26*, 373–381.
31. Zhang, X.T.; Yang, S.D. *Introduction to Regional Geology of Qinghai Province*; Geological Press: Beijing, China, 2007; pp. 36–39.
32. Wang, Y.Z.; Bai, Y.S.; Lu, H.L. Geological characteristics of Tianjunnanshan ophiolite in Qinghai and its forming environment. *Qinghai Geol.* **2001**, *1*, 29–35.
33. Guo, A.L.; Zhang, G.W.; Sun, Y.G.; Cheng, S.Y.; Yao, A.P. Geochemistry and spatial distribution of Late Paleozoic mafic volcanic rocks in the surrounding areas of the Gonghe basin—The implication from Maji mountain triple junction and East Paleo-Tethys archipelago ocean. *Sci. China Ser. D Earth Sci.* **2007**, *S1*, 249–261.
34. Guo, A.L.; Zhang, G.W.; Sun, Y.G.; Cheng, S.Y.; Qiang, J. Sr-Nd-Pb isotopic geochemistry of late-Paleozoic mafic volcanic rocks in the surrounding areas of the Gonghe basin, Qinghai province and geological implications. *Acta Petrol. Sin.* **2007**, *23*, 747–754.
35. Guo, A.L.; Zhang, G.W.; Qiang, J.; Sun, Y.G.; Li, G.; Yao, A.P. Indosinian Zongwulong orogenic belt on the northeastern margin of the Qinghai-Tibet plateau. *Acta Petrol. Sin.* **2009**, *25*, 1–12.
36. Peng, Y. The Late Hercynian-Indosinian Structural Characteristics of the Zongwulong Tectonic Belt in North Qaidam Basin. Ph.D. Thesis, Chinese Academy of Geological Sciences, Beijing, China, 2015.
37. Wu, C.L.; Lei, M.; Wu, D.; Li, T.X. Zircon SHRIMP Dating and Genesis of Granites in Wulan Area of Northern Qaidam. *Acta Geosci. Sin.* **2016**, *37*, 493–516.
38. Wu, C.L.; Wu, D.; Mattinson, C.; Lei, M.; Chen, H.J. Petrogenesis of granitoids in the Wulan area: Magmatic activity and tectonic evolution in the North Qaidam, NW China. *Gondwana Res.* **2019**, *67*, 147–171. [[CrossRef](#)]
39. Cheng, T.T. Zircon U-Pb Dating and Tectonic Setting of Intrusive Rocks in Wulan along the North Margin of Qaidam Terrane. Master's Thesis, Hefei University of Technology, Hefei, China, 2015.
40. Wang, Y.S.; Niu, M.L.; Li, X.C.; Wu, Q.; Han, Y.; Zhao, Q.Q.; Da, L.C. LA-ICP-MS Zircon U-Pb Dating and Petrogenesis of the Quartz-Diorites from the Guokeshan Area in the Northern Margin of the Qaidam Basin. *Acta Geol. Sin.* **2017**, *91*, 94–110. [[CrossRef](#)]
41. Niu, M.L.; Zhao, Q.Q.; Wu, Q.; Li, X.C.; Yan, Z.; Li, J.L.; Sun, Y.; Yuan, X.Y. Magma mixing identified in the Guokeshan pluton, northern margin of the Qaidam basin: Evidences from petrography, mineral chemistry, and whole-rock geochemistry. *Acta Petrol. Sin.* **2018**, *34*, 1991–2016.
42. Zhang, J.P.; Niu, M.L.; Li, C.; Li, X.C.; Sun, Y.; Yuan, X.Y.; Wang, L. Petrogenesis and Implications of Late Permian-Middle Triassic granites in Wulan area, the eastern segment of the North Qaidam tectonic belt. *Chin. J. Geol.* **2022**, *57*, 1103–1129.
43. Li, H.R.; Qian, Y.; Sun, F.Y.; Wang, Y.Z. Paleozoic to Mesozoic magmatism in North Qaidam, Qinghai Province, NW China: Implications for tectonic evolution. *Gondwana Res.* **2023**, *115*, 37–56. [[CrossRef](#)]
44. Pin, C.; Paquette, J.L. A mantle derived bimodal suite in the Hercynian belt: Nd isotope and trace element evidence for a subduction—Related rift origin of the late Devonian Brevenne metavolcanics, Massif Central (France). *Contrib. Mineral. Petrol.* **1997**, *129*, 222–238. [[CrossRef](#)]
45. Pin, C.; Marini, F. Early Ordovician continental break-up in Variscan Europe: Nd-Sr isotope and trace element evidence from bimodal igneous associations of the southern Massif Central, France. *Lithos* **1993**, *29*, 177–196. [[CrossRef](#)]
46. Geist, D.; Howard, K.A.; Larson, P. The generation of oceanic rhyolites by crystal fractionation: The basalt-rhyolite association at Volcan Alcedo, Galapagos Archipelago. *J. Petrol.* **1995**, *36*, 965–982. [[CrossRef](#)]
47. Bonin, B. Do coeval mafic and felsic magmas in post-collisional to within-plate regimes necessarily imply two contrasting, mantle and crustal, sources? A review. *Lithos* **2004**, *78*, 1–24. [[CrossRef](#)]
48. Espinoza, F.; Morata, D.; Polvé, M.; Lagabrielle, Y.; Maury, R.C.; Guivel, C.; Cotton, J.; Bellon, H.; Suárez, M. Bimodal back-arc alkaline magmatism after ridge subduction: Pliocene felsic rocks from Central Patagonia (47°S). *Lithos* **2008**, *101*, 191–217. [[CrossRef](#)]

49. Wang, X.L.; Shu, L.S.; Xing, G.F.; Zhou, J.C.; Tang, M.; Shu, X.J.; Qi, L.; Hu, Y.H. Post-orogenic extension in the eastern part of the Jiangnan orogen: Evidence from ca 800–760 Ma volcanic rocks. *Precambrian Res.* **2012**, *222–223*, 404–423. [[CrossRef](#)]
50. Guo, P.Y.; Niu, Y.L.; Sun, P.; Wang, X.H.; Gong, H.M.; Duan, M.; Zhang, Y.; Kong, J.J.; Tian, L.Y.; Wu, S.G. The Early Cretaceous bimodal volcanic suite from the Yinshan Block, western North China Craton: Origin, process and geological significance. *J. Asian Earth Sci.* **2018**, *160*, 348–364. [[CrossRef](#)]
51. Davies, J.; von Blanckenburg, F. Slab break off: A model of lithosphere detachment and its test in the magmatism and deformation of collisional orogens. *Earth Planet. Sci. Lett.* **1995**, *129*, 85–102. [[CrossRef](#)]
52. Bird, P. Continental delamination and the Colorado Plateau. *J. Geophys. Res.* **1979**, *84*, 7561–7571. [[CrossRef](#)]
53. Gao, S.; Jin, Z.M. Delamination and its dynamic significance of crust–mantle evolution. *Geol. Sci. Technol. Inf.* **1997**, *16*, 3–11.
54. Schott, B.; Schmeling, H. Delamination and detachment of a lithospheric root. *Tectonophysics* **1998**, *296*, 225–247. [[CrossRef](#)]
55. England, P.; Houseman, G. Extension during continental convergence, with application to the Tibetan Plateau. *J. Geophys. Res. Solid Earth* **1989**, *94*, 17561–17579. [[CrossRef](#)]
56. Lu, S.N. *Preliminary Study on Precambrian Geology in the Northern Qinghai-Tibetan Plateau*; Geology Press: Beijing, China, 2002; pp. 1–125.
57. Song, S.G.; Zhang, L.F.; Niu, Y.L. Ultra-deep origin of garnet peridotite from the North Qaidam ultrahigh-pressure belt, northern Tibetan Plateau, NW China. *Am. Mineral.* **2004**, *89*, 1330–1336. [[CrossRef](#)]
58. Song, S.G.; Zhang, L.F.; Niu, Y.L.; Su, L.; Jian, P.; Liu, D.Y. Geochronology of diamond bearing zircons from garnet peridotite in the North Qaidam UHPM belt, northern Tibetan Plateau: A record of complex histories from oceanic lithosphere subduction to continental collision. *Earth Planet. Sci. Lett.* **2005**, *234*, 99–118. [[CrossRef](#)]
59. Wang, H.C. Early Paleozoic Collisional Orogeny and Magmatism on Northern Margin of the Qaidam Basin. Ph.D. Thesis, China University of Geosciences (Beijing), Beijing, China, 2006.
60. Lu, Z.L.; Zhang, J.X.; Mao, X.H.; Zhou, G.S.; Teng, X.; Wu, Y.W. Ordovician adakite-Nb-enriched basalt suite in the eastern North Qaidam Mountains: Implications for oceanic subduction and crustal accretion prior to deep continental subduction. *Acta Petrol. Sin.* **2020**, *36*, 2995–3017.
61. Gong, S.L.; Chen, N.S.; Wang, Q.Y.; Kusky, T.M.; Wang, L.; Zhang, L.; Ba, J.; Liao, F.X. Early Paleoproterozoic magmatism in the Quanji Massif, northeastern margin of the Qinghai-Tibet Plateau and its tectonic significance: LA-ICPMS U-Pb zircon geochronology and geochemistry. *Gondwana Res.* **2012**, *21*, 152–166. [[CrossRef](#)]
62. Gong, S.L.; He, C.; Wang, X.C.; Chen, N.S.; Kusky, T. No plate tectonic shutdown in the early Paleoproterozoic: Constraints from the ca. 2.4 Ga granitoids in the Quanji Massif, NW China. *J. Asian Earth Sci.* **2019**, *172*, 221–242. [[CrossRef](#)]
63. Song, S.G.; Zhang, G.B.; Zhang, C.; Zhang, L.F.; Wei, C.J. The dynamic process of oceanic subduction and continental collision: The petrological constraints of the HP-UHP metamorphic belt in the North Qilian-North Qaidam. *Chin. Sci. Bull.* **2013**, *58*, 2240–2245.
64. He, C.; Gong, S.L.; Wang, L.; Chen, N.S.; Santosh, M.; Wang, Q.Y. Protracted post-collisional magmatism during plate subduction shutdown in early Paleoproterozoic: Insights from post-collisional granitoid suite in NW China. *Gondwana Res.* **2018**, *55*, 92–111. [[CrossRef](#)]
65. Niu, M.L.; Cai, Q.R.; Li, X.C.; Yakymchuk, C.; Wu, Q.; Yuan, X.Y.; Sun, Y. Early Paleozoic tectonic transition from oceanic to continental subduction in the North Qaidam tectonic belt: Constraints from geochronology and geochemistry of syncollisional magmatic rocks. *Gondwana Res.* **2021**, *91*, 58–80. [[CrossRef](#)]
66. Sun, J.P.; Chen, S.Y.; Peng, Y.; Shao, P.C.; Ma, S.; Liu, J. Determination of Early Cambrian Zircon SHRIMP U-Pb Datings in Zongwulong Tectonic Belt, Northern Margin of Qaidam Basin, and Its Geological Significance. *Geol. Rev.* **2015**, *61*, 743–752.
67. Wang, Q.Y.; Chen, N.S.; Li, X.Y.; Hao, S.; Chen, H.H. LA-ICP-MS zircon U-Pb geochronological constraints on the tectonothermal evolution of the Early Paleoproterozoic Dakendaban Group in the Quanji Block, NW China. *Chin. Sci. Bull.* **2008**, *53*, 2849–2858.
68. Sun, J.P.; Chen, S.Y.; Peng, Y.; Ma, S.; Shao, P.C.; Liu, J. Early Neoproterozoic Glacier Event in Oulongbuluke Block: Evidence from CIA Index. *Geol. Rev.* **2016**, *62*, 29–36.
69. Lu, S.N.; Li, H.K.; Zhang, C.L.; Niu, G.H. Geological and geochronological evidence for the Precambrian evolution of the Tarim Craton and surrounding continental fragments. *Precambrian Res.* **2008**, *160*, 94–107. [[CrossRef](#)]
70. Yuan, G.B.; Wang, H.C.; Li, H.M.; Hao, G.J.; Xin, H.T.; Zhang, B.H.; Wang, Q.H.; Tian, Q. Zircon U-Pb age of the Gabbros in Lvliangshan Area on the Northern Margin of Qaidam Basin and its Geological Implication. *Geol. Surv. Res.* **2002**, *25*, 36–40.
71. Zhang, J.X.; Christopher, G.; Meng, F.C. Polyphase tectonothermal history recorded in granulitized gneisses from the North Qaidam HP/UHP metamorphic terrane, Western China: Evidence from zircon U-Pb geochronology. *Geol. Soc. Am. Bull.* **2008**, *120*, 732–749. [[CrossRef](#)]
72. Zhang, C.; Zhang, L.F.; Roermund, H.V.; Song, S.G.; Zhang, G.B. Petrology and SHRIMP U-Pb dating of Xitieshan eclogite, North Qaidam UHP metamorphic belt, NW China. *J. Asian Earth Sci.* **2011**, *42*, 752–767. [[CrossRef](#)]
73. Lu, L.; Wu, Z.H.; Hu, D.G.; Barosh, P.J.; Hao, S.; Zhou, C.J. Zircon U-Pb age for rhyolite of the Maoniushan Formation and its tectonic significance in the East Kunlun Mountains. *Acta Petrol. Sin.* **2010**, *26*, 1150–1158.
74. Zhang, Y.L.; Hu, D.G.; Shi, Y.R.; Lu, L. SHRIMP zircon U-Pb ages and tectonic significance of Maoniushan Formation volcanic rocks in East Kunlun orogenic belt, China. *Geol. Bull. China* **2010**, *29*, 1614–1618.
75. Zhang, Y.L.; Ni, J.Y.; Shen, Y.X.; Wang, C.Q.; Gao, W.L.; Hu, D.G. Zircon U-Pb Ages and Geological Significance of Volcanic Rocks from Maoniushan Formation in the Northern Margin of Qaidam Basin. *Geoscience* **2018**, *32*, 329–334.

76. Hu, J.; Lu, Y.; Xiao, X.Q.; Zeng, J.; Luo, B. Geochemical Characters and Geological Implications of Volcanic Rocks from Maoniushan Formation in Amunick Mountain of Northern Qaidam. *Northwestern Geol.* **2016**, *49*, 73–83.
77. Qi, X.P.; Yang, J.; Fan, X.G.; Wang, B.Y. Chronology and Geochemistry of the Dacite in the Maoniushan Formation in Eastern Part of the Eastern Kunlun Orogen. *Bull. Mineral. Petrol. Geochem.* **2018**, *37*, 482–494.
78. Li, R.B.; Pei, X.Z.; Li, Z.C.; Patias, D.; Su, Z.G.; Pei, L.; Chen, G.C.; Chen, Y.X.; Liu, C.J. Late Silurian to Early Devonian volcanics in the East Kunlun orogen, northern Tibetan Plateau: Record of postcollisional magmatism related to evolution of the Proto-Tethys Ocean. *J. Geodyn.* **2020**, *140*, 101780. [[CrossRef](#)]
79. Fu, C.L.; Yan, Z.; Wang, Z.Q.; Buckman, S.; Aitchison, J.C.; Niu, M.L. Lajishankou ophiolite complex: Implications for Paleozoic multiple accretionary and collisional events in the South Qilian belt. *Tectonics* **2019**, *37*, 1321–1346. [[CrossRef](#)]
80. Sun, J.P.; Dong, Y.P.; Ma, L.C.; Chen, S.Y.; Jiang, W. Devonian to Triassic tectonic evolution and basin transition in the East Kunlun-Qaidam area, northern Tibetan Plateau: Constraints from stratigraphy and detrital zircon U-Pb geochronology. *GSA Bull.* **2022**, *134*, 1967–1993. [[CrossRef](#)]
81. Tan, X.J.; Wang, Z.M. General High-Pressure Closed Acidic Decomposition Method of Rock Samples for Trace Element Determination Using Inductively Coupled Plasma Mass Spectrometry. *J. Anal. Chem.* **2020**, *75*, 1295–1303.
82. Chen, F.K.; Hegner, E.; Todt, W. Zircon ages and Nd isotopic and chemical compositions of orthogneisses from the Black Forest, Germany: Evidence for a Cambrian magmatic arc. *Int. J. Earth Sci.* **2000**, *88*, 791–802. [[CrossRef](#)]
83. Li, H.K.; Geng, J.Z.; Hao, S.; Zhang, Y.Q.; Li, H.M. Determination of U-Pb isotopic age of zircon by Laser Ablation Inductively Coupled Plasma Mass Spectrometer (LA-ICP-MS). *Acta Miner. Sin.* **2009**, *29*, 600–601.
84. Yuan, H.L. State Key Laboratory of Continental Dynamics, Northwest University. *Rock Miner. Anal.* **2012**, *31*, 1090–1092.
85. Hoskin, P.W.O.; Schaltegger, U. The composition of zircon and igneous and metamorphic petrogenesis. *Rev. Mineral. Geochem.* **2003**, *53*, 27–55. [[CrossRef](#)]
86. Wu, Y.B.; Zheng, Y.F. Genetic mineralogy of zircon and its constraints on U-Pb age interpretation. *Chin. Sci. Bull.* **2004**, *49*, 1589–1604. [[CrossRef](#)]
87. Moller, A.; O'Brien, P.J.; Kennedy, A.; Kroner, A. Linking growth episodes of zircon and metamorphic textures to zircon chemistry: An example from the ultrahigh-temperature granulites of Rogaland (SW Norway). *EMU Notes Mineral.* **2003**, *5*, 65–82. [[CrossRef](#)]
88. Wilson, M. *Igneous Petrogenesis*; Unwin Hyman: London, UK, 1989; pp. 1–366.
89. Irvine, I.N.; Baragar, W.R.A. A Guide to Chemical Classification of the Common Volcanic Rocks. *Can. J. Earth Sci.* **1971**, *8*, 523–548. [[CrossRef](#)]
90. Condie, K.C. Geochemical changes in basalts and andesites across the Archean-Proterozoic boundary—Identification and significance. *Lithos* **1989**, *23*, 1–18. [[CrossRef](#)]
91. Frey, F.A.; Green, D.H.; Roy, S.D. Integrated models of basalt petrogenesis: A study of quartz tholeiites to olivine melilitites from South Eastern Australia utilizing geochemical and experimental Petrological data. *J. Petrol.* **1978**, *19*, 463–513. [[CrossRef](#)]
92. Sun, S.S.; McDonough, W.F. Chemical and isotopic systematics of oceanic basalts: Implications for mantle composition and processes. *Magmatism in Ocean Basins. Geol. Soc. Lond. Spec. Public* **1989**, *42*, 313. [[CrossRef](#)]
93. Rudnick, R.L.; Gao, S. Composition of the Continental Crust. In *The Crust*; Rudnick, R.L., Ed.; Elsevier-Pergamon: Oxford, UK, 2003; pp. 1–64.
94. Ewart, A.; Milner, S.C.; Armstrong, R.A.; Dungan, A.R. Etendeka volcanism of the Goboboseb Mountains and Messum igneous complex, Namibia. Part I: Geochemical evidence of Early Cretaceous Tristan plume melts and the role of crustal contamination in the Paraná-Etendeka CFB. *J. Petrol.* **1998**, *39*, 191–225. [[CrossRef](#)]
95. Ewart, A.; Marsh, J.S.; Milner, S.C.; Duncan, A.R.; Kamber, B.S.; Armstrong, R.A. Petrology and geochemistry of Early Cretaceous bimodal continental flood volcanism of the NW Etendeka, Namibia. Part 1: Introduction, mafic lavas and re-evaluation of mantle source components. *J. Petrol.* **2004**, *45*, 59–105. [[CrossRef](#)]
96. Peng, Y.; Ma, Y.S.; Liu, C.L.; Li, Z.X.; Sun, J.P.; Shao, P.C. Geological characteristics and tectonic significance of the Indosinian granodiorites from the Zongwulong tectonic belt in North Qaidam. *Earth Sci. Front.* **2016**, *23*, 206–221.
97. Kou, G.C.; Feng, J.W.; Luo, B.R.; Zhou, W.G.; Liu, S.Q. Zircon U-Pb dating and geochemistry of the volcanic rocks from Maoniushan Formation in Amunike area, Qinghai Province, and its geological implications. *Geol. Bull. China* **2017**, *36*, 275–284.
98. Li, J.B.; Wan, S.C.; Li, Z.H. Geological and Geochemistry Characteristics of Volcanics in the Late Paleozoic Maoniushan Formation in Amunike Area of Northern Qaidam Basin. *Northwestern Geol.* **2017**, *50*, 47–53.
99. Wang, Z.L. Geochemistry and Genesis of Maoniushan Formation Volcanic Rocks in Amunick, Qinghai Province. Master's Thesis, Chengdu University of Technology, Chengdu, China, 2017.
100. Yang, Z.Z.; Sun, J.; Zhao, X.K.; Tian, Z.; Zhao, Z.Y.; Sun, D.L.; Li, D.L.; Yang, B.Z.; Yang, Q.S. LA-ICP-MS U-Pb Age of the Zircons from the Volcanic Rocks in Maoniushan Formation in Shidiquan Area, Delingha, Qinghai, and Its Geological Significance. *Geol. Rev.* **2017**, *63*, 1613–1623.
101. Feng, Q.; Qin, Y.; Fu, S.T.; Liu, Y.Q.; Zhou, D.W.; Ma, D.D.; Wang, L.Q.; Ren, J.H.; Wang, C.Y. U-Pb Age of Detrital Zircons and Its Geological Significance from Maoniushan Formation in the Wulan County, Northern Margin of Qaidam Basin. *Acta Sedimentol. Sin.* **2015**, *33*, 486–499.
102. MacLean, W.H. Mass change calculations in altered rock series. *Miner. Depos.* **1990**, *25*, 44–49. [[CrossRef](#)]
103. MacLean, W.H.; Barrett, T.J. Lithochemical techniques using immobile elements. *J. Geochem. Explor.* **1993**, *48*, 109–133. [[CrossRef](#)]

104. Wang, Y.X.; Gu, X.L.; Zhang, S.Z.; Wu, C.Z.; Zhang, K.J.; Li, H.M.; Yang, J.D. Geochronology and Nd-Sr-Pb isotops of the bimodal volcanic rocks of the Bogda rift. *Acta Petrol. Sin.* **2006**, *22*, 1215–1224.
105. Tao, G.H.; Li, X.F.; Chen, W.L.; Chen, W.; Lu, G.; Hao, C.; Pan, S.; Wu, K.N. Geochemistry of Devonian bimodal volcanic rocks in Yemaquan area, Inner Mongolia, and their implications for the early Paleozoic tectonic evolution in Beishan area. *Geol. Bull. China* **2020**, *41*, 1783–1797.
106. Wang, Y.L.; Li, J.C.; Han, W.X.; Wang, W.Z. The principle of discriminating the composition of mantle-derived magma source and the nature of Emeishan mantle source. *Acta Geol. Sin.* **1993**, *67*, 52–62.
107. Pearce, J.A. Trace elements characteristics of lavas from destructive plate boundaries. In *Andesites: Orogenic Andesites and Related Rocks*; Thorpe, R.S., Ed.; Wiley: Chichester/London, UK, 1982; pp. 525–548.
108. Rapp, R.P.; Shimizu, M.D. Norman Growth of early continental crust by partial melting of eclogite. *Nature* **2003**, *425*, 605–609. [[CrossRef](#)]
109. Xia, L.Q.; Xia, Z.C.; Xu, X.Y.; Li, X.M.; Ma, Z.P. Mid-Late Neoproterozoic rift-related volcanic rocks in China: Geological records of rifting and break-up of Rodinia. *Geosci. Front.* **2012**, *3*, 375–399. [[CrossRef](#)]
110. Shervais, J.W. Ti-V plots and the petrogenesis of modern and ophiolitic lavas. *Earth Planet. Sci. Lett.* **1982**, *59*, 101–108. [[CrossRef](#)]
111. Lassiter, J.C.; DePaolo, D.J. Plume/lithosphere interaction in the generation of continental and oceanic flood basalts: Chemical and isotopic constraints. In *Largeigneous Provinces: Continental, Oceanic, and Planetary Flood Volcanism*; Mahoney, J., Coffin, M.F., Eds.; Geophysical Monograph; American Geophysical Union: Washington DC, USA, 1997; pp. 335–355.
112. Niu, Y.L.; Collerson, K.D.; Batiza, R.; Wendt, J.I.; Regelous, M. Origin of enriched-type mid ocean ridge basalt at ridges far from mantle plumes: The East Pacific Rise at 11°20' N. *J. Geophys. Res.* **1999**, *4*, 7067–7087. [[CrossRef](#)]
113. Bacon, C.; Drit, T.H. Compositional evolution of the zoned calc-alkaline magma chamber of Mount Mazama, Crater Lake, Oregon. *Contrib. Mineral. Petrol.* **1988**, *98*, 224–256. [[CrossRef](#)]
114. Christiansen, R.L. Yellowstone magmatic evolution: Its bearing on understanding large-volume explosive volcanism. In *Explosive Volcanism: Inception, Evolution and Hazards*; National Academy Press: Washington, DC, USA, 1984; pp. 84–95.
115. Beard, J.S. Experimental, geological, and geochemical constraints on the origins of low-K silicic magmas in oceanic arcs. *J. Geophys. Res. Atmos.* **1995**, *100*, 15593–15600. [[CrossRef](#)]
116. Liu, S.B.; Li, J.B.; Li, Y.P.; Li, D.S.; Zhang, A.K.; He, S.Y. Geochemical Characteristics of the Volcanic Rocks from the Maoniushan Formation in the Dadakenwulashan Pb-Zn Deposit, East Kunlun and Its Significance. *Northwestern Geol.* **2016**, *49*, 11–24.
117. Taylor, S.R.; McLennan, S.M. The geochemical evolution of the continental crust. *Rev. Geophys.* **1995**, *33*, 241–265. [[CrossRef](#)]
118. Kerrich, R.; Polat, A.; Wyman, D.; Hollings, P. Trace element systematics of Mg-, to Fe-tholeiitic basalt suites of the Superior Province: Implications for Archean mantle reservoirs and greenstone belt genesis. *Lithos* **1999**, *46*, 163–187. [[CrossRef](#)]
119. Jung, S.; Pfänder, J.A. Source composition and melting temperatures of orogenic granitoids: Constraints from CaO/Na₂O, Al₂O₃/TiO₂ and accessory mineral saturation thermometry. *Eur. J. Mineral.* **2007**, *19*, 859–870. [[CrossRef](#)]
120. Whalen, J.B.; Currie, K.L.; Chappell, B.W. A-type granites: Geochemical characteristics, discrimination and petrogenesis. *Contrib. Miner. Petrol.* **1987**, *95*, 405–419. [[CrossRef](#)]
121. Eby, G.N. Chemical subdivision of the A-type granitoids: Petrogenesis and tectonic implications. *Geology* **1992**, *20*, 641–644. [[CrossRef](#)]
122. Pearce, J.A.; Lippard, S.J.; Roberts, S. Characteristics and tectonic significance of supra-subduction zone ophiolites. *Geol. Soc. Lond. (Spec. Publ.)* **1984**, *16*, 77–94. [[CrossRef](#)]
123. Zhu, Y.H.; Lin, Q.X.; Jia, C.X.; Wang, G.C. SHRIMP zircon U-Pb age and significance of Early Paleozoic volcanic rocks in East Kunlun orogenic belt, Qinghai Province, China. *Sci. China Earth Sci.* **2006**, *49*, 88–96. [[CrossRef](#)]
124. Kaygusuz, A.; Siebel, W.; Ilbeyli, N.; Arslan, M.; Satir, M.; Sen, C. Insight into magma genesis at convergent plate margins: A case study from the eastern Pontides (NE Turkey). *J. Mineral. Geochem.* **2010**, *187*, 265–287. [[CrossRef](#)]
125. Boztuğ, D.; Harlavan, Y.; Arehart, G.B.; Satir, M.; Avci, N. K-Ar age, whole-rock and isotope geochemistry of A-type granitoids in the Divriği-Sivas region, eastern-central Anatolia, Turkey. *Lithos* **2007**, *97*, 193–218. [[CrossRef](#)]
126. Coulon, C.; Maluski, H.; Bollinger, C.; Wang, S. Mesozoic and Cenozoic volcanic rocks from central and southern Tibet: ³⁹Ar/⁴⁰Ar dating, petrological characteristics and geodynamic significance. *Earth Planet. Sci. Lett.* **1986**, *79*, 281–302. [[CrossRef](#)]
127. Hochstaedter, A.G.; Gill, J.B.; Kusakabe, M.; Newman, S.; Pringle, M.; Taylor, B.; Fryer, P. Volcanism in the Sumisu Rift, I. Major element, volatile and stable geochemistry. *Earth Planet. Sci. Lett.* **1990**, *100*, 179–194. [[CrossRef](#)]
128. Hochstaedter, A.G.; Gill, J.B.; Morris, J. Volcanism in the Sumisu Rift, II. Subduction and non-subduction related components. *Earth Planet. Sci. Lett.* **1990**, *100*, 195–209. [[CrossRef](#)]
129. Wang, Y.; Qian, Q.; Liu, L.; Zhang, Q. Main characteristics of bimodal volcanic rocks in different tectonic settings. *Acta Petrol. Sin.* **2000**, *16*, 169–173.
130. Xia, L.Q.; Xia, Z.C.; Xu, X.Y.; Li, X.M.; Ma, Z.P. The discrimination between continental basalt and island arc basalt based on geochemical method. *Acta Petrol. Mineral.* **2007**, *26*, 77–88.
131. Wang, Y.L.; Zhang, C.J.; Xiu, S.Z. The Th/Hf-Ta/Hf discrimination diagram of geotectonic setting of basalts. *Acta Petrol. Sin.* **2001**, *17*, 413–421.
132. Zhang, G.B.; Song, S.G.; Zhang, L.F.; Niu, Y.L. The subducted oceanic crust within continental-type UHP metamorphic belt in the North Qaidam, NW China: Evidence from petrology, geochemistry and geochronology. *Lithos* **2008**, *104*, 99–108. [[CrossRef](#)]

133. Zhu, X.H.; Chen, D.L.; Wang, C.; Wang, H.; Liu, L. The Initiation, Development and Termination of the Neoproterozoic-Early Paleozoic Ocean in the Northern Margin of Qaidam Basin. *Acta Geol. Sin.* **2015**, *89*, 234–250.
134. Dong, Y.P.; Zhang, G.W.; Hauzenberger, C.; Neubauer, F.; Yang, Z.; Liu, X.M. Palaeozoic tectonics and evolutionary history of the Qinling orogen: Evidence from geochemistry and geochronology of ophiolite and related volcanic rocks. *Lithos* **2011**, *122*, 39–56. [[CrossRef](#)]
135. Dong, Y.P.; Santosh, M. Tectonic architecture and multiple orogeny of the Qinling Orogenic Belt, Central China. *Gondwana Res.* **2016**, *29*, 1–40. [[CrossRef](#)]
136. Dong, Y.P.; He, D.F.; Sun, S.S.; Liu, X.M.; Zhou, X.H.; Zhang, F.F.; Yang, Z.; Cheng, B.; Zhao, G.C.; Li, J.H. Subduction and accretionary tectonics of the East Kunlun orogen, western segment of the Central China Orogenic System. *Earth-Sci. Rev.* **2018**, *186*, 231–261. [[CrossRef](#)]
137. Dong, Y.P.; Sun, S.S.; Liu, X.M.; He, D.F.; Zhou, X.H.; Zhang, F.F.; Yang, Z.; Zhou, D.W. Geochronology and geochemistry of the Yazidaban ophiolitic melange in Qimantagh: Constraints on the Early Paleozoic back-arc basin of the East Kunlun Orogen, northern Tibetan Plateau. *J. Geol. Soc. Lond.* **2019**, *176*, 306–322. [[CrossRef](#)]
138. Li, R.B.; Pei, X.Z.; Li, Z.C.; Pei, L.; Chen, G.C.; Wei, B.; Chen, Y.X.; Liu, C.J.; Wang, M. Cambrian (–510 Ma) ophiolites of the East Kunlun orogen, China: A case study from the Acite ophiolitic tectonic mélange. *Int. Geol. Rev.* **2018**, *60*, 2063–2083. [[CrossRef](#)]
139. Pei, X.Z.; Li, R.B.; Li, Z.C.; Liu, C.J.; Chen, Y.X.; Pei, L.; Liu, Z.Q.; Chen, G.C.; Li, X.B.; Wang, M. Composition Feature and Formation Process of Buqingshan Composite Accretionary Mélange Belt in Southern Margin of East Kunlun Orogen. *Earth Sci.* **2018**, *43*, 4498–4520.
140. Ren, L.; Liang, H.Y.; Bao, Z.W.; Zhang, J.; Li, K.X.; Huang, W.T. The petrogenesis of early Paleozoic high-Ba-Sr intrusions in the North Qinling terrane, China, and tectonic implications. *Lithos* **2018**, *314–315*, 534–550. [[CrossRef](#)]
141. Song, S.G.; Niu, Y.L.; Su, L.; Xia, X.H. Tectonics of the North Qilian orogen, NW China. *Gondwana Res.* **2013**, *23*, 1378–1401. [[CrossRef](#)]
142. Song, S.G.; Bi, H.Z.; Qi, S.S.; Yang, L.M.; Allen, M.B.; Niu, Y.L.; Su, L.; Li, W.F. HP-UHP Metamorphic Belt in the East Kunlun Orogen: Final Closure of the Proto-Tethys Ocean and Formation of the Pan-North-China Continent. *J. Petrol.* **2018**, *59*, 2043–2060. [[CrossRef](#)]
143. Xiao, W.J.; Windley, B.F.; Yong, Y.; Yan, Z.; Yuan, C.; Liu, C.Z.; Li, J.L. Early Paleozoic to Devonian multiple accretionary model for the Qilian Shan, NW China. *J. Asian Earth Sci.* **2009**, *35*, 323–333. [[CrossRef](#)]
144. Yang, J.S.; Xu, Z.Q.; Ma, C.Q.; Wu, C.L.; Zhang, J.X.; Wang, Z.Q.; Wang, G.C.; Zhang, H.F.; Dong, Y.P.; Lai, S.C. Compound orogeny and scientific problems concerning the Central Orogenic Belt of China. *Geol. China* **2010**, *37*, 1–11.
145. Zhang, G.W.; Zhang, B.R.; Yuan, X.C.; Xiao, Q.H. *Qinling Orogenic Belt and Continental Dynamics*; Science Press: Beijing, China, 2001; pp. 1–855.
146. Yang, J.S.; Xu, Z.Q.; Zhang, J.X.; Zhang, Z.M.; Liu, F.L.; Wu, C.L. Tectonic setting of main high-and ultrahigh-pressure metamorphic belts in China and adjacent region and discussion on their subduction and exhumation mechanism. *Acta Petrol. Sin.* **2009**, *25*, 1529–1560.
147. Xia, L.Q.; Li, X.M.; Yu, J.Y.; Wang, G.Q. Mid-Late Neoproterozoic to Early Paleozoic volcanism and tectonic evolution of the Qilian Mountain. *Geol. China* **2016**, *43*, 1087–1138.
148. Yu, S.Y.; Peng, Y.B.; Zhang, J.X.; Li, S.Z.; Santosh, M.; Li, Y.S.; Liu, Y.J.; Gao, X.Y.; Ji, W.T.; Lv, P.; et al. Tectono-thermal evolution of the Qilian orogenic system: Tracing the subduction, accretion and closure of the Proto-Tethys Ocean. *Earth-Sci. Rev.* **2021**, *215*, 103574. [[CrossRef](#)]
149. Han, Y.S.; Peng, C. Geological characteristics of Tuomuerrite Ophiolite mélange belt and its tectonic significance. *Qinghai Inst. Geol. Surv.* **2000**, *1*, 18–25.
150. Shi, R.D.; Yang, J.S.; Wu, C.L. First SHRIMP dating for the formation of the late Sinian Yushigou ophiolite North Qilian Mountains. *Acta Geol. Sin.* **2004**, *78*, 649–657.
151. Wu, C.L.; Yang, J.S.; Xu, Z.Q.; Wooden, J. Granitic Magmatism on the Early Paleozoic UHP Belt of Northern Qaidam, NW China. *Acta Geol. Sin.* **2004**, *78*, 658–674.
152. Zhu, X.H.; Chen, D.L.; Liu, L.; Wang, C.; Yang, W.Q.; Cao, Y.T.; Kang, L. Chronology and geochemistry of the mafic rocks in Xitieshan area, North Qaidam. *Geol. Bull. China* **2012**, *31*, 2079–2089.
153. Song, S.G.; Yang, L.M.; Zhang, Y.Q.; Niu, Y.L.; Wang, C.; Su, L.; Gao, Y.L. Qi-Qin accretionary belt in Central China Orogen: Accretion by trench jam of oceanic plateau and formation of intra-oceanic arc in the Early Paleozoic Qin-Qi-Kun Ocean. *Sci. Bull.* **2017**, *62*, 1038. [[CrossRef](#)]
154. Yang, L.M.; Song, S.G.; Su, L.; Allen, M.B.; Niu, Y.L.; Zhang, G.B.; Zhang, Y.Q. Heterogeneous oceanic arc volcanic rocks in the South Qilian accretionary belt (Qilian Orogen, NW China). *J. Petrol.* **2019**, *60*, 85–116. [[CrossRef](#)]
155. Wen, T.; Song, S.G.; Wang, C.; Allen, M.B.; Dong, J.; Feng, D.; Su, L. IBM type forearc magmatism in the Qilian Orogen records evolution from a continental to an intra-oceanic arc system in the Proto-Tethyan Ocean. *Gondwana Res.* **2022**, *110*, 197–213. [[CrossRef](#)]
156. Li, R.B.; Pei, X.Z.; Pei, L.; Li, Z.C.; Chen, G.C.; Chen, Y.X.; Liu, C.J.; Wang, M. The Early Triassic Andean-type Halagatu granitoid pluton in the East Kunlun orogen, northern Tibet Plateau: Response to the northward subduction of the Paleo-Tethys Ocean. *Gondwana Res.* **2018**, *62*, 212–226. [[CrossRef](#)]

157. Li, R.B.; Pei, X.Z.; Li, Z.C.; Pei, L.; Chen, G.C.; Liu, Z.Q.; Chen, Y.X.; Liu, C.J.; Wang, M.; Zhang, M. Paleo-Tethyan Ocean Evolution and Indosinian Orogenesis in the East Kunlun Orogen, Northern Tibetan Plateau. *Minerals* **2022**, *12*, 1590. [[CrossRef](#)]
158. Li, R.B.; Pei, X.Z.; Zhou, R.J.; Li, Z.C.; Pei, L.; Chen, G.C.; Chen, Y.X.; Liu, C.J. Magmatic response to the closure of the Proto-Tethys Ocean: A case study from the middle Paleozoic granitoids in the Kunlun Orogen, western China. *J. Asian Earth Sci.* **2023**, *242*, 105513. [[CrossRef](#)]
159. Sun, Y.G.; Zhang, G.W.; Wang, J.; Zhan, F.T.; Zhang, Z.Y. $^{40}\text{Ar}/^{39}\text{Ar}$ Age of the Basic Sill Swarms of Two Periods in the Junction Area of Qinling and Kunlun and Its Tectonic Significance. *Acta Geol. Sin.* **2004**, *78*, 65–71.
160. Chen, M.; Xue, C.J.; Xue, W.W.; Zhao, W.T. Discovery and geological significance of Xuji diorite in Zongwulong tectonic belt on the northern margin of Qaidam Basin. *Acta Petrol. Mineral.* **2020**, *39*, 552–568.
161. Chen, L.; Sun, Y.; Pei, X.Z.; Gao, M.; Feng, T.; Zhang, Z.Q.; Chen, W. ^{40}Ar - ^{39}Ar age of the Derni ophiolite: Evidence for the existence and extension of the Paleo-Tethys Ocean basin at the northernmost end of the Qinghai-Tibet Plateau. *Chin. Sci. Bull.* **2001**, *46*, 424–426.
162. Yang, J.S.; Wang, X.B.; Shi, R.D.; Xu, Z.Q.; Wu, C.L. Derni ophiolite at the southern margin of the East Kunlun orogen in the northern Qinghai-Tibet Plateau: A dismembered Paleo-Tethys oceanic crust. *Geol. China* **2004**, *31*, 225–239.
163. Ye, Z.F.; Wang, J.; Wang, B.Z.; Suo, Y.X.; Song, T.Z.; Ma, Y.S. The Discovery and preliminary study of the early Devonian strata in the Bukadabanfeng area in the central and western segment of the East Kunlun Orogen. *Northwestern Geol.* **2004**, *37*, 13–18.
164. Zhang, Z.Y.; Yin, H.F.; Wang, B.Z.; Wang, J.; Zhang, K.X. Presence and Evidence of Kuhai-Saishitang Branching Ocean in Copulae between Kunlun-Qinling Mountains. *Earth Sci.* **2004**, *29*, 691–696.
165. Kay, R.W.; Kay, S.M. Delamination and delamination magmatism. *Tectonophysics* **1993**, *219*, 177–189. [[CrossRef](#)]
166. Sacks, P.E.; Secor, D.T., Jr. Delamination in collisional orogens. *Geology* **1990**, *18*, 999–1002. [[CrossRef](#)]
167. Nelson, K.D. Are crustal thickness variations in old mountain belts like the Appalachians a consequence of lithospheric delamination? *Geology* **1992**, *20*, 498–502. [[CrossRef](#)]
168. Seber, D.; Barazangi, M.; Ibrahimi, A.; Demnati, A. Geophysical evidence for lithospheric delamination beneath the Alboran Sea and Rif-Betic mountains. *Nature* **1996**, *379*, 785–790. [[CrossRef](#)]
169. Watson, E.B.; Harrison, T.M. Zircon saturation revisited: Temperature and composition effects in a variety of crustal magma types. *Earth Planet. Sci. Lett.* **1983**, *64*, 295–304. [[CrossRef](#)]
170. Frost, C.D.; Frost, B.R. Reduced rapakivi-type granites: The tholeiite connection. *Geology* **1997**, *25*, 647–650. [[CrossRef](#)]
171. King, P.L.; White, A.J.R.; Chappell, B.W.; Allen, C.M. Characterization and origin of aluminous A-type granites from the Lachlan Fold Belt, southeastern Australia. *J. Petrol.* **1997**, *38*, 371–391. [[CrossRef](#)]

Disclaimer/Publisher's Note: The statements, opinions and data contained in all publications are solely those of the individual author(s) and contributor(s) and not of MDPI and/or the editor(s). MDPI and/or the editor(s) disclaim responsibility for any injury to people or property resulting from any ideas, methods, instructions or products referred to in the content.